# Alternative activation of mast cells by CD4$^+$ T helper cells

**Edouard Leveque,[1,2] Louise Battut,[2,3] Camille Petitfils, [2,3] Salvatore Valitutti,[1,4] Nicolas Cenac,[2,3] Gilles Dietrich[2,3], Eric Espinosa[2,3,*]**

[1]Toulouse Institute for Infectious and Inflammatory Diseases (Infinity), INSERM UMR1291, CNRS UMR5051, Toulouse, France.

[2]Toulouse University, Université Paul Sabatier, Toulouse, F-31062, France

[3]Inserm, U1220, Institut de Recherche en Santé Digestive (IRSD), INRA, INP-ENVT, Toulouse, F-31024, France

[4]Department of Pathology, Institut Universitaire du Cancer-Oncopole de Toulouse, CHU Toulouse, 31059 Toulouse, France.

*Correspondence*

Eric Espinosa

eric.espinosa@inserm.fr

INSERM U1220

Institut de Recherche en Santé Digestive (IRSD)

CHU Purpan, Place du Dr Baylac

CS 60039

31024 Toulouse cedex 3 - France

Email: eric.espinosa@inserm.fr

*Disclosures*

The authors declare no competing interest

# Abstract

Effector $CD4^+$ T lymphocytes (Teff) infiltrate sites of inflammation and orchestrate the immune response by instructing local leukocytes. Mast cells (MCs) are tissue sentinel cells strategically located near blood vessels and T cell rich areas. MC/Teff cells interactions shape Teff cell responses but in turn, Teff cell action on MC is still poorly understood. Here, we analyzed the human MC/Teff cells interplay through both the application of RNAseq and functional assays. We showed that activated Teff cells induce a specific transcriptomic program in MCs including production of both inflammatory cytokines and chemokines, prostaglandin, and a FcεRI-dependent degranulation facilitation thereby driving them toward an inflammatory phenotype. Moreover, Teff cells induce in MCs the capacity to interact with $CD4^+$ T cell through a wide-range of dedicated soluble and membrane ligands and to play the role of antigen presenting cells (APCs).



*Keywords*

Mast cells, helper T cells, Cell-cell communication, eicosanoids, IFN-γ


*Summary sentence*

Effector $CD4^+$ T lymphocytes endow mast cells with antigen presenting cell and pro-inflammatory capabilities

*Abbreviations*

APC, antigen presenting cell; COX, cyclo-oxygenase, DAMP, damage-associated molecular pattern; FC, fold change; IFN, interferon; MC, mast cell, $MC^{Teff}$ (MCs cocultured with activated $CD4^+$ memory T cells); Teff, Effector T lymphocytes; TF, transcription factor; TPM (Transcripts Per Kilobase Million)

# 1 Introduction

Mast cells (MCs) are tissue resident innate immune cells particularly abundant in skin and mucosa. MC response to innate stimuli (complement component C5a, alarmins such as IL-33) or antibody-targeted antigens are well-documented [1-3]. According to their triggered receptors, MCs swiftly release numerous prestored mediators by degranulation or *de novo* synthesize cytokines, chemokines and eicosanoids [1, 4]. They participate for instance to inflammatory response initiation, defense against pathogens, venom detoxification, tissue repair or immune response regulation [2, 5].

A strategic location nearby blood vessels and the ability to produce a vast array of chemokines, such as CCL1, CCL4, CCL5 allow MCs to participate in leucocyte recruitment and to interact with infiltrated cells. Effector $CD4^+$ T cells (Teff) differentiated in the secondary lymphoid organs circulate in the blood and infiltrate inflamed tissues where they need to be stimulated by local antigen presenting cells (APCs) to produce cytokines and chemokines [6-9]. Locally activated Teff cells deliver several cues that drive tissue responses and notably influence the response of local innate immune cells such as macrophages or dendritic cells [10-12]. MCs can produce several T cell chemo-attractants and MC/T cell close contacts were often reported [13-15] suggesting MC/infiltrating Teff cell interplay. The MC to $CD4^+$ T cell communication axis was documented in several reports notably showing that MCs can mold Th cell responses [13, 16-18]. Under certain conditions, human and mouse MCs can serve as APCs and form immunological synapses with $CD4^+$ T cells to drive T cell cytokine production [17, 19, 20]. On the other hand, $CD4^+$ Teff cell to MC communication axis is less documented. *In vitro* and *in vivo* experimental evidences indicated that $CD4^+$ T cells can activate MCs [13, 21-24]. We and other showed that in some circumstances direct contact between MCs and T cells was needed to activate MCs [14, 25, 26] while other studies showed a distant action via vesicle or soluble mediators [23]. Nevertheless, a more comprehensive view of the action of Teff cell on MCs is still missing.

To explore the extent of Teff cell impact on MCs and its peculiarity, we examined the profile of primary human MCs following interaction with activated $CD4^+$ Teff cells or stimulation with canonical MC stimuli such as IgE/Ag or IL-33 using deep RNA-sequencing and mass spectrometry. We found that MCs cocultured with activated $CD4^+$ Teff cells (referred to here as $MC^{Teff}$) upregulate a typical set of highly wired genes promoted notably by IFN-$\gamma$ that endows MCs with inflammatory and APC capabilities.

# 2 Methods

## 2.1 Key resources table (see supplemental data)

## 2.2 Resource availability

### *2.2.1 Lead contact*

Further information and requests for resources and reagents should be directed to and will be

fulfilled by the lead contact, Eric Espinosa (eric.espinosa@inserm.fr).

### *2.2.2 Materials availability*

This study did not generate new unique reagents.

## 2.3 Human primary MC cultures

Peripheral blood mononuclear cells (PBMCs) were isolated from buffy coats from anonymous healthy volunteer donors (aged 18-60 years) provided by the French Blood Establishment (EFS, Toulouse, France). $CD34^+$ precursors cells were isolated from PBMCs (EasySep™ Human CD34 Positive Selection Kit, STEMCELL Technologies). $CD34^+$ cells were grown under serum-free conditions using StemSpan™ medium (STEMCELL Technologies) supplemented with recombinant human IL-6 (50 ng/mL; Peprotech), human IL-3 (10 ng/mL; Peprotech) and 3% supernatant of CHO transfectants secreting murine SCF (a gift from Dr. P. Dubreuil, Marseille, France, 3% correspond to ~50 ng/mL SCF) for one week. Cells were next grown in IMDM Glutamax I, sodium pyruvate, 2-mercaptoethanol, 0.5% BSA, Insulin-transferrin selenium, Penicillin/Streptomycin (100 U/mL / 100 µg/mL) (all from Invitrogen), IL-6 (50 ng/mL) and 3% supernatant of CHO transfectants secreting murine SCF for 8 weeks and tested phenotypically ($Tryptase^+$, $CD117^+$, $Fc\varepsilon RI^+$) and functionally (β-hexosaminidase release in response to FcεRI crosslinking) before use for experiments. Only primary cell lines showing more than 95% $CD117^+/Fc\varepsilon RI^+$ cells were used for experiments.

## 2.4 coculture experiments

$1 \times 10^5$ memory $CD4^+$ T cells freshly purified from PBMC by negative selection and magnetic separation (EasySep™ Human memory $CD4^+$ T cell enrichment kit, STEMCELL Technologies) were cocultured at 1:1 ratio with non-autologous human primary MCs for 24 hours with or without anti-CD3/CD28–coated beads (Dynabeads, Life Technologies) at 1 bead:10 T cells ratio in RPMI 1640 supplemented with 10% serum replacement medium (knockout medium, Life Technologies), GlutaMAX-I, sodium pyruvate, 2-mercaptoethanol, and 1% supernatant of CHO transfectants secreting murine SCF (coculture medium).

## 2.5 Confocal microscopy

MCs and memory $CD4^+$ T cells were cocultured (ratio 1:1) for two days with or without anti-CD3/28 coated beads in coculture medium. Cells were washed in PBS and beads were removed using a magnet. Cells were next pulsed with a cocktail of superantigens (SEA, SEB, TSST-1, 50 ng/mL) in coculture medium for 1 hour at 37°C. Cells were washed and $2x10^5$ cells were mixed with $1x10^5$ resting memory $CD4^+$ T cells (from the same donor as the previous T cells and stained with CFSE (Invitrogen) according to the Manufacturer's recommendations) in 200 µL coculture medium in 96-wells U-bottom plate. Cells were spun at 40 g to allow conjugate formation and incubated at 37°C for 2.5 hours. Cells were transferred onto poly-L-lysine–coated slides and next fixed (4% PFA for 15 min.), permeabilized (PBS, 1% BSA, 5% FCS, 0.1% saponin), and stained with anti-IFN-γ mAb (Clone B27, BD-Pharmingen) followed by secondary Abs (Goat anti-mouse-Alexa 555) in PBS 1% BSA, 5% FCS, 0.1% saponin and next counterstained with DAPI (1 µg/mL, Invitrogen). The samples were mounted and examined with the use of a Zeiss LSM 710 confocal microscope with a 20X or 63X Plan-Apochromat objective (1.4oil), electronic zoom 3. Scoring of the slides was performed in a blinded fashion by evaluating for each condition at least 100 conjugates in randomly selected fields from 3 independent experiments.

## 2.6 MC degranulation assay

MCs were sensitized with anti-DNP human IgE (1 µg/mL, Sigma-Aldrich) for 16 hours and next cocultured with memory $CD4^+$ T cells (ratio 1:1) with or without anti-CD3/28 coated beads for 48 hours. Cells were washed in Tyrode' Buffer and distributed in 96-well flat-bottom plate in 50 µL Tyrode's buffer and adapted to 37°C for 20 minutes. MCs were then treated with 50 µL of DNP-BSA (Thermo Fisher Scientific) for 45 min at 37°C. MC degranulation was assessed by CD63 exposure assay and by β-hexosaminidase assay. Cells were stained with anti-CD63-FITC mAb (H5C6) at 4°C for 30 min and proceeded to flow cytometry analysis. β-hexosaminidase release was quantified by spectrophotometric analysis of the hydrolysis of p-nitrophenyl-N-acetyl-β-D-glucosaminide (PNAG, Sigma-Aldrich) in 0.1 M sodium citrate buffer (pH 4.5). 20 µL of cell supernatant or whole cell lysate (cells were lysed with 1% Triton X100) were incubated with PNAG for 45 min. at 37°C and reaction was stopped with 150µL glycine buffer (0.4M, pH 10.7). Absorbance at 405 nm was measured using a Multiskan Ascent plate reader. The activity in the whole cell lysate was referred to as 100%.

## 2.7 transwell assay

Transwell inserts (Corning Cat. No. 3413) with polycarbonate 6.5 mm membrane diameter and 0.4 µm pore size were used to separate MCs (upper compartment) and memory $CD4^+$ T

cells stimulated with anti-CD3/CD28 coated beads (lower compartment). Cells were cocultured separated or not with transwell inserts for 48 hours. Eicosanoids were quantified in the cell pellets by LC-MS/MS.

## 2.8 PUFA metabolites LC-MS/MS measurements

PUFA metabolites were extracted from the cell pellets following the methods previously described [27]. 6-keto-prostaglandin F1 alpha (6kPGF1$\alpha$), thromboxane B2 (TxB2), $PGE_2$, 8-iso$PGA_2$, $PGE_3$, 15d-$PGJ_2$, $PGD_2$, lipoxin A4 (LxA4), LxB4, 7-Maresin 1 (7-Mar1), leukotriene B4 ($LtB_4$), $LtB_5$, protectin Dx (PDx), 18-hydroxyeicosapentaenoic (18-HEPE), 9-hydroxyoctadecadienoic acid (9-HODE), 13-HODE, 15-hydroxyeicosatetraenoic acid (15-HETE), 12-HETE, 8-HETE, 5-HETE, 17-hydroxydocosahexaenoic acid (17-HDoHE), 14-HDoHE, 14,15-epoxyeicosatrienoic acid (14,15-EET), 11,12-EET, 8,9-EET, 5,6-EET, and 5-oxoeicosatetraenoic acid (5-oxoETE) were quantified. To simultaneously separate 27 lipids of interest and three deuterated internal standards (5-HETEd8, LxA4d4 and LtB4d4), LC-MS/MS analysis was performed on an ultrahigh-performance liquid chromatography system (UHPLC; Agilent LC1290 Infinity) coupled to an Agilent 6460 triple quadrupole MS (Agilent Technologies) equipped with electrospray ionization operating in negative mode. Reverse-phase UHPLC was performed using a ZorBAX SB-C18 column (Agilent Technologies) with a gradient elution. The mobile phases consisted of water, acetonitrile (ACN), and formic acid (FA) [75:25:0.1 (v/v/v)] (solution A) and ACN and FA [100:0.1 (v/v)] (solution B). The linear gradient was as follows: 0% solution B at 0 min, 85% solution B at 8.5 min, 100% solution B at 9.5 min, 100% solution B at 10.5 min, and 0% solution B at 12 min. The flow rate was 0.35 ml/min. The autosampler was set at 5°C, and the injection volume was 5 µL. Data were acquired in multiple reaction monitoring (MRM) mode with optimized conditions. Peak detection, integration, and quantitative analysis were performed with MassHunter Quantitative analysis software (Agilent Technologies). For each standard, calibration curves were built using 10 solutions at concentrations ranging from 0.95 to 500 ng/ml. A linear regression with a weight factor of 1/X was applied for each compound. The limit of detection (LOD) and the limit of quantification (LOQ) were determined for the 28 compounds using signal-to-noise (S/N) ratios. The LOD corresponded to the lowest concentration leading to an S/N value >3, and LOQ corresponded to the lowest concentration leading to an S/N value >10. All values less than the LOQ were not considered. Blank samples were evaluated, and their injection showed no interference (no peak detected), during the analysis.

## 2.9 Flow cytometry and cell sorting

Cell surface staining with fluorochrome-labelled primary Abs were performed in PBS 1% FCS 1% human serum (HS) at the concentration recommended by the manufacturer at 4°C for 30 min. Cell viability was ascertained by labeling with fixable viability dyes (eBioscience).

For intracellular CXCL9 and CXCL10 staining, MCs and $CD4^+$ memory T cells were cocultured for 48 h and GolgiPlug™ was added 4 hours before the end of the coculture. Cells were washed in PBS and incubated with anti-CD117 (104D2) mAb and viability dye (eBioscience™ Fixable Viability Dye eFluor™ 780) in PBS 1% FCS 1% HS at 4°C for 30 min. Cells were washed in PBS and next fixed in PFA 4% for 10 min. at RT and permeabilized with PBS 1% FCS 1% HS 0.1 % saponin (permeabilization buffer) for 10 min. Cells were next incubated with anti-CXCL9 (J1015E10) and CXCL10 (J034D6) mAbs in permeabilization buffer for 45min at RT. Cells were next washed in PBS and proceeded to flow cytometry analysis.

All flow cytometry experiments were acquired using a custom configuration Fortessa flow cytometer and the FACS Diva software (BD Biosciences) and analyzed with FlowJo V10.4.2 software (TreeStar). Cell sorting was performed by using a custom configuration FACSAria cell sorter (BD Biosciences) or FACSMelody cell sorter (BD biosciences). MCs and $CD4^+$ memory T cells in cocultures were sorted as $SSC^{high}$ $CD117^+$ and $SSC^{low}$ $CD117^-$ cells respectively.

## 2.10 Cytokine quantitation

For CXCL-9 and CXCL-10 quantitation, coculture supernatants were collected after 48h and stored at -80°C. Cytokine concentrations were measured by bead-based multiplex assay (LEGENDplex™, Biolegend) according to the Manufacturer's recommendations. Flow cytometric analysis were performed with a MACSQuant® Analyzer 10 instrument (Miltenyi Biotec).

## 2.11 RNAseq Libraries Preparation

750 000 MCs were either FACS-sorted after 24h of coculture with resting or anti-CD3/28 coated beads-activated memory $CD4^+$ T cells or stimulated or not for 4 hours with 10 ng/mL of IL-33 (Peprotech) or with 100 ng/mL of DNP-BSA (thermo-fischer scientific). We used a longer stimulation time for coculture to give the $CD4^+$ T cells time to activate and then stimulate MCs. RNA was extracted using miRNeasy Mini Kit (Qiagen). Libraries were prepared using 1 µg of high-quality total RNA. TruSeq stranded mRNA Library prep kit (Illumina) and Truseq RNA Unique Dual Indexed Adapters (Illumina) are used according to the manufacturer protocol. Size selection was performed using AMPure XP beads (Beckman

Coulter). Library size and quality were confirmed on Fragment analyzer (Agilent). Libraries were quantified by qPCR using the KAPA quantification kit for Illumina platforms (KAPA Biosystems, Roche). Samples were pooled in equimolar fashion. The libraries were sequenced on a NextSeq 550 (Illumina) in pair end sequencing 2 × 75 bp with dual indexes (i7 and i5, 8bp).

## 2.12 RNAseq Analysis

Read alignment and gene quantification for RNA-seq: FastQ files were generated via llumina bcl2fastq2 (version 2.20.0.422). Cutadapt 4.0 (Galaxy Version 4.0+galaxy1) was used to trim the reads (minimum length=20 and quality cutoff=10). Reads were next mapped to the human (hg38) Galaxy built-in reference genome with RNA STAR (Galaxy Version 2.7.10b+galaxy3 and default parameters) using Ensembl GRCh38.p13 (v106) annotation file. Mapped reads were counted using the featureCounts function of Rsubread (v2.12.3) package [28]. FPKM (Fragments Per Kilobase of transcript per Million mapped reads) and TPM (Transcripts Per Kilobase Million) values were calculated using edgeR package function *rpkm* with featureCounts output.

Differential analyses of RNA-Seq data at the gene level were performed using the DESeq2 R package (v1.38.3) with the recommended workflow [29]. Venn diagrams were generated using eulerr (v7.0.0) R package. DEG adjusted p-values (FDR) and $\log_2$ fold changes were displayed as volcano plots using EnhancedVolcano (v 1.16.0) R package. For visualization and clustering (PCA, heatmaps of sample-to-sample distances), regularized logarithm (rlog) transformation of the count data was performed to remove the dependence of the variance on the mean. R Pheatmap package (v1.0.12) was used to display DEGs (hierarchical clustering using the euclidean distance and complete linkage method). Heatmaps for specific groups of genes were generated using R package ComplexHeatmap (v 2.6.2) to visualize both genes clustered by expression and $\log_2$ fold change plus TPM values [30]. Functional enrichment analysis were performed with the Bioconductor package ReactomePA [31] and *enrichPathway* function (FDR<0.01) or via STRING database v11 (https://string-db.org/). Cytoscape v3.9.1 was used to represent PPI networks using STRING application. PPI of upregulated or downregulated DEGs were analyzed for experimentally validated interactions, with a combined score of > 0.7 indicating a high confidence score for significant interaction.

## 2.13 Weighted gene co-expression network analysis - WGCNA

The *vst* (variance-stabilizing transformation) function from the DESeq2 R package was used to normalize and transform the raw count data. The top 40% of genes (6487 genes) with the largest variance were selected for WGCNA. The weighted gene co-expression network was

constructed by WGCNA (v1.72-1) R package following authors' workflow [32]. Soft thresholding power β (to which co-expression similarity is raised to calculate adjacency) was chosen based on the criterion of approximate scale-free topology by using *pickSoftThreshold* function. β=28 resulted in a scale-free topology fit index $R^2$ of 0.88 (Figure S1A-B), implying the biological relevance of the network. Automatic network construction and module detection function *blockwiseModules* was used to generate a signed network with β=28, a minimum module size of 30, a mergeCutHeight threshold for merging of modules of 0.2 and a medium sensitivity (deepSplit=2) to cluster splitting. The 30 resulting gene modules were assigned with different color names by the software (unassigned genes were given grey color).

Eigengene for each module (first principal component of the expression matrix of the corresponding module) was used to compute module-stimulation condition associations and detect modules uniquely associated with + $T_{ACT}$ coculture condition. A heatmap plot of yellow module gene expressions by stimulation conditions associated to the corresponding module eigengene (barplot) (Figure S1C) was constructed.

Gene correlation with each module (goodness of fit of each gene to its module is assessed using the signed eigengene connectivity measure kME) that represents module membership was calculated by correlating its gene expression profile with the module eigengene with kME table. Correlation with yellow module was used to rank the genes inside the yellow module and genes showing a high correlation (>0.8) were selected for functional enrichment analysis and ChIP-X Enrichment Analysis Version 3 (ChEA3) database (https://maayanlab.cloud/chea3/) was used to identify the candidate transcription factors that regulate these genes. ChEA3 identifies the transcription factors most likely to explain the expression of a set of target genes according to an integrated scoring across multiple information sources for potential regulatory activity, including ENCODE and ReMap ChIP-seq experiments.

## 2.14 Overlap between $MC^{Teff}$ upregulated genes and disease-associated genes

We used the GWAS catalog (https://www.ebi.ac.uk/gwas/home) to obtain mapped gene lists associated to traits (we chose several typical IMID and non-IMID such as infectious diseases, allergy and cancers). Summary statistics were downloaded from the NHGRI-EBI GWAS Catalog [33]. Gene-disease association with p-value < $5.10^{-8}$ (widely used to identify association between a common genetic variant and a trait of interest) were kept for the overlap analysis. $MC^{Teff}$ upregulated genes and disease-associated gene lists were

compared using the GeneOverlap R package (v 1.26.0). GeneOverlap performs Fisher's exact test to test the significance of each pair of gene list overlap in comparison with a genomic background (21,196 human genes). The function returns the number of common genes between the two lists, the P value, and the estimated odds ratio. Odds ratio larger than 1 indicate a positive association between lists. The overlap between lists was represented by plotting odds ratios, P values and the number of common genes for each disease.

### 2.15 Quantitative real-time PCR in MC/T cell cocultures for RNA-seq validation

RNA extracted for RNAseq Libraries preparation was also employed for RT-qPCR analysis (RNAseq validation). Reverse transcription of total RNA was performed using the SuperScript™ VILO™ cDNA Synthesis Kit according to the manufacturer's recommendations (thermo Fisher scientific). real-time PCR was performed with Master Mix Fast Advanced TaqMan™ (Thermofisher Scientific) using a StepOnePlus™ Real-Time PCR detection system (Applied Biosystems™). Following primers were used: IL13 (Hs00174379_m1), CCL4 (Hs99999148_m1), ERN1 (Hs00980095_m1), Gene expression was normalized as n-fold difference to the housekeeping gene GAPDH (Hs03929097_g1) based on the $2^{-\Delta\Delta Ct}$ method. Relative quantification of gene expression was performed with the StepOne Software v2.3 (Applied Biosystems™).

### 2.16 Statistical Analysis

Statistical tests were performed with Graph Pad Prism V9 software (GraphPad Software, Inc.). Test performed are indicated in the figure legends. Non parametric tests were performed when group distribution failed normality or variance homogeneity. All p values are two-sided, (* $p < 0.05$; ** $p < 0.01$; *** $p < 0.001$; **** $p < 0.0001$ and ns, not significant).

# 3 Results

## 3.1 Activated $CD4^+$ Teff cells induce a specific activation program in mast cells

MCs are tissue resident cells strategically located near blood vessels that can interact with infiltrating $CD4^+$ Teff cells in an antigen-independent manner. To mimic this situation and analyze the effects of activated $CD4^+$ Teff cells on MCs, freshly isolated human memory $CD4^+$ T cells were cocultured with non-autologous primary human MCs for 24 hours with or without anti-CD3/CD28 coated beads. In parallel experiments, MCs were stimulated with two

typical well-known MC stimuli (IL-33 and IgE/Ag) as points of comparison (Figure 1A). MCs were then FACS-sorted and processed to mRNA deep sequencing (RNAseq).

Principal component analysis (PCA) showed that whilst MC coculture with unstimulated T cells did not impact MC transcriptomic signature, activated memory $CD4^+$ T cells induced a clear shift in gene expression segregated from the other stimulated conditions (Figure 1B). The non-supervised clustering of the 500 most variable genes clearly identified +IL-33, +IgE/Ag and $+T_{ACT}$ conditions and showed that a group of genes is specifically upregulated upon coculture with activated memory $CD4^+$ T cells (Figure 1C). Of note, gene-expression data obtained by RNA-seq correlated with RT-qPCR measurements (Figure S2).

The analysis of differentially expressed genes (DEGs) between stimulated MCs and resting MCs indicated that activated memory T cells (+ $T_{ACT}$ condition) induced the regulation of a substantial number of genes with respectively 609 and 240 strongly (Fold Change, FC>3) upregulated and downregulated genes (Figure 1D). Proportional-area Venn diagrams overlapping-based analysis of DEGs showed that while some DEGs are shared between the three stimulation conditions, 523 upregulated genes and 316 downregulated genes appeared specific to $+T_{ACT}$ condition (Figure 1E). To note, resting memory $CD4^+$ T cells did not change the transcriptomic profile of MCs ($+T_{CTRL}$ vs unstimulated MC condition, Figure 1B-D) indicating that resting $CD4^+$ T cells are unable to activate MCs. This basic analysis suggests that activated $CD4^+$ T cells induce changes in the transcription of a large number of genes in MCs, more than half of which are not transcriptionally impacted following activation by classical stimuli such as IgE/Ag or IL-33.

These observations prompted us to deepen our analysis by performing Weighted Gene Correlation Network Analysis (WGCNA) on the entire gene expression dataset. We used this unsupervised method to group genes that behave similarly across the different stimulation conditions and search whether some highly interconnected genes (clustered in modules) were related to $+T_{ACT}$ stimulation condition. 30 co-expression modules were identified by using a dynamic tree cutting algorithm (Figure 2A). Eigengene module which summarizes the expression profiles of the genes inside a single module [34] was next used to associate modules to stimulation condition. We observed that some modules were associated with one or more stimulation conditions. We identified one module (yellow) of 607 genes (Table S1) whose high expression level is uniquely associated with the $+T_{ACT}$ condition (Figure 2B and S2C). To note, 76% of these genes were upregulated with fold change>2 in $+T_{ACT}$ condition according to the differential gene expression analysis (Table S1). We next analyzed the 446 yellow module genes showing high (>0.8) correlation (eigengene-based connectivity) with this module. Pathway over-representation analysis using Reactome database indicated that

they were involved in response to interferons, antiviral defense and complement system. (Figure 2C). Transcription factor enrichment analysis (Figure 2D) was performed using ChIP-X Enrichment Analysis 3 (ChEA3) web-sever which integrates a collection of gene set libraries generated from multiple sources including TF-gene co-expression, TF-target associations, and TF-gene co-occurrence [35]. Transcription factors related to interferon response such as STAT1, STAT2 and IRFs were the most enriched.

Taken together these results show that activated $CD4^+$ Teff cells trigger in MCs a large set off genes. Among them, we identified a network of upregulated genes, not shared with IgE/Ag- or IL-33-induced activation. These genes are mainly related to IFN-γ-induced immune functions such as antigen presentation, complement system and defense to viruses.

## 3.2 MC Transcriptional program induced by activated memory $CD4^+$ T cells

To have a global view of $MC^{Teff}$ DEGs, we compared conditions in which MC were incubated with activated or resting memory $CD4^+$ T cells. This analysis resulted in 1652 DEGs (|Fold Change|>2 and FDR<0.01) (Figure 3A). Among them, 945 were upregulated and 707 downregulated (table S2). To gain insight into the 945 upregulated DEGs, we first mapped them against their expression level (low: TPM<10; intermediate 10<TPM<100 and strong, TPM>100), their expression fold change and their predicted location (“predicted secreted proteins” and “cell surface proteins” for protein coding genes) by using Human Protein Atlas database (proteinatlas.org) [36]. Published literature was next scoured to identify bona fide secretory proteins (table S2). We next mapped them to the Search Tool for Retrieval of Interacting Genes (STRING v11.5, https://string-db.org) [37] to acquire protein–protein interaction (PPI) networks. Among these 945 upregulated DEGs, 736 code for proteins and 383 of them form a highly connected network (PPI enrichment p.value<$10^{-16}$) using high confidence level of 0.7. Markov clustering (MCL) algorithm (based on the distance matrix obtained from the STRING global scores) was used to identify functional gene groups in this network. Five main subnetworks were identified (Figure 3B). Gene ontology analysis of these networks using STRING (GO biological processes) pointed out that three of them are tightly related to IFN response (including IFN-γ signaling, defense to viruses and antigen presentation via MHC class I and II molecules) and gather several genes identified using WGCNA (Table S2). The other two are related to cytokine response and NFκB signaling.

To further determine whether known immune-related pathways were over-represented among all upregulated DEGs, we ran pathway Over-Representation Analysis using the Reactome database [38] and showed that intercellular communication and antigen

presentation-associated pathways were enriched (Figure 3C). Enrichment analysis using KEGG database confirmed these results and suggested a relation between upregulated DEGs and IMIDs (Immune-mediated inflammatory diseases) such as autoimmune thyroid disease or type I diabetes mellitus (Figure S3A). This observation prompted us to test whether upregulated DEGs significantly overlapped with gene sets associated to different type of pathologies obtained in the NHGRI-EBI GWAS Catalog [33]. We included in this analysis pathologies exemplifying four classes of diseases (IMID, infectious, cancer and allergic) and observed that $MC^{Teff}$ DEGs significantly overlapped mostly with IMID-associated genes (figure S3B).

A similar analysis was conducted with the 707 downregulated DEGs. Among them, 453 coded for proteins and only 75 are involved in a poorly interconnected PPI network (STRING analysis with high confidence score of 0.7) (Table S2 and Figure S4A). Pathway over representation analysis showed a poor enrichment in specific pathways and indicated a relation to extracellular matrix degradation or adhesion (Figure S4B).

Taken together these results indicated that Teff cells induce in MCs the expression of genes mainly associated with immune regulatory processes and antigen processing and presentation.

### 3.3 Teff cells induce an APC phenotype in MCs

Because these results suggested that, in turn, $MC^{Teff}$ upregulated genes involved in antigen presentation, we analyzed the potential of $MC^{Teff}$ to provide ligands involved in immunological synapse formation with activated $CD4^+$ T cells. To this end, we defined a set of canonical genes coding for molecules involved in signal 1 and 2 provided by APCs to $CD4^+$ T cells according to the literature [39, 40] (Figure S5). $MC^{Teff}$ gene expression analysis showed that the majority of genes coding key molecules involved in the immunological synapse were upregulated and expressed with a transcripts per kilobase million (TPM) >10 (Figure 4A). We confirmed by flow cytometry analysis that MHC class II and costimulation molecules (ex: CD80, PD-L1 and ICAM-1) were expressed at the $MC^{Teff}$ surface after 48h of coculture (Figure 4B). To go further, we investigated whether $MC^{Teff}$ were able to fully activate memory $CD4^+$ T cells upon cognate interaction. Since activated lymphocytes express MHC class II molecules and are capable of self-presenting antigen [41, 42], we used a special experimental design to answer this question. $MC^{Teff}$ were generated by coculture with activated memory $CD4^+$ T cells and pulsed with a bacterial superantigen cocktail (Toxic shock syndrome toxin-1, TSST-1 and staphylococcal enterotoxin A and B, SEA, SEB, able to activate more than 50% of a polyclonal human $CD4^+$ T cell population [43]) and incubated

with resting memory $CD4^+$ T cells labelled with CFSE to distinguish them from their counterparts. To demonstrate unambiguously that $MC^{Teff}$ present superantigens, we analyzed the formation of functional immunological synapses where $CFSE^+$ lymphocyte exhibited IFN-γ polarization toward conjugated APC [44, 45]. Confocal microscopy analysis showed that $MC^{Teff}$ were able to form functional immunological synapses with resting $CFSE^+$ $CD4^+$ memory T cells (Figure 4C). Quantification of $MC^{Teff}$ conjugated with $CFSE^+$ IFN-$\gamma^+$ $CD4^+$ T cells showed that about 25% of CFSE+ T cells conjugated with $MC^{Teff}$ formed functional immunological synapses (Figures 4-D and S5). Of note, we chose to analyze IFN-γ production because Th1 are the most frequent Teff cells in a polyclonal CD4+ T cell population and unlike other cytokines, its secretion is polarized [45]. These data show that superantigen-induced cognate $MC^{Teff}$-resting memory CD4+ T cell interaction leads to full T cell activation. Collectively, these results indicate that Teff cells make the MCs capable of providing memory $CD4^+$ T cells with key signals 1 and 2.

### 3.4 Activated Teff cells promote the secretion of pro-inflammatory mediators in MCs.

We next sought immune related effector molecules secreted by $MC^{Teff}$. We focused on the 32 upregulated DEGs coding secreted proteins with strong or intermediate expression fold change (FC>3) and expression level (TPM>10) with known immune functions (table S2). We used STRING to acquire protein–protein interaction (PPI) networks. Two main networks were identified (Figure 5A) including mainly cytokines, chemokines and antimicrobial/pro-inflammatory molecules (complement components, Pentraxine 3). Interestingly, the upregulated chemokine set (CXCL9, CXCL10, CCL1, CCL3 and CCL4) was mainly dedicated to T cell attraction via CXCR3, CCR8 and CCR5. Both CXCL9 and CXCL10 were detected in the supernatant of MC/activated Teff cell coculture (Figure 5B). Because activated memory $CD4^+$ T cells upregulate also *CXCL9* and *CXCL10* gene expression (according to RNAseq data [46]) we analyzed CXCL9 and CXCL10 production by flow cytometry after coculture (Figure 5 C-D). We observed that activated Teff cells induced a population of $CXCL9^+$ and $CXCL10^+$ MCs. Several cytokine-coding genes were upregulated in $MC^{Teff}$ (Table S2 and Figure 5A). At the protein level, we analyzed key cytokines associated to inflammatory response and known to drive Th cell polarization. TNF, IL-6 and IL-1β production was increased in MCs/Teff cells cocultures (Figure 5D). Both IL-12 and IL-23 were not detected. Accordingly, RNAseq analysis showed that MCs did not express *IL12B*, coding for IL-12 p40 subunit shared by IL-12 and IL-23 cytokines, in any of the conditions tested.

$MC^{Teff}$ also upregulated diverse genes coding immune regulatory processes (grey color in figure 5A) such as *ISG15* coding an ubiquitin-like protein that also functions extracellularly by signaling through LFA-1 in T and NK lymphocytes to promote IFN-γ secretion [47]. Secreted N-myc and STAT interactor (NMI) and interferon-induced protein 35 (IFP35) play the role of DAMPs [48]. On the other hand, IL-18 binding protein, Interleukin-4–induced gene 1 (IL4I1) and galectin 9 are negative immune regulators.

### 3.5 Activated Teff cells potentiate MC degranulation and induce eicosanoid production.

We next investigated whether activated $CD4^+$ T cells influence key MC functions such as degranulation and eicosanoid production. Anti-DNP IgE sensitized MCs were cocultured with $CD4^+$ T cells with or without anti-CD3/CD28 coated beads for 48 hours and next challenged with DNP-BSA for 30 minutes. MC degranulation measured either with CD63 cell surface exposure or β-hexosaminidase release assays indicated that MCs showed a decreased FcεRI activation threshold and an increased degranulation capacity when cocultured with activated Teff cells (Figure 6A-B). The analysis of 27 polyunsaturated fatty acid metabolites by liquid chromatography coupled to tandem mass spectrometry [27] showed that when MCs were cocultured with activated Teff cells, only COX-dependent eicosanoids were increased (Thromboxane $B_2$, Prostaglandin $E_2$ ($PGE_2$), $PGD_2$, 8-iso$PGA_2$, 15d-$PGJ_2$) (Figure 6C).

Because both effector $CD4^+$ T cells and MCs are able to produce eicosanoids, we quantified eicosanoids in each cell type isolated by FACS cell sorting (Figure 6D). Eicosanoids increased in coculture condition were mainly detected in MCs compared to activated $CD4^+$ T cells; only very low amounts of some lipid mediators (e.g., $TxB_2$ and $PGD_2$) were found in T cells (Figure 6D). These results indicated that activated Teff cells triggered COX-dependent eicosanoids production in MCs. Similar coculture experiments performed with Transwell system showed that $PGE_2$, $PGD_2$, 15d-$PGJ_2$ production required direct contact between MCs and $CD4^+$ T cells whereas $TxB_2$ production was contact-independent (Figure 6E).

The inducible key rate-limiting enzyme in prostanoid synthesis, COX-2, being not upregulated in $MC^{Teff}$ (Table S2), we analyzed the expression levels of genes coding for enzymes directly involved in $PGE_2$ metabolism as well as MIR155, a regulator of this pathway [49]. Our analysis indicated that $PGE_2$ production in $MC^{Teff}$ may be dependent on both the up regulation of prostaglandin E synthases (PTGES2/3) and a downregulation of catabolic enzymes such as HPGR1 and HPGR2 (Figure 6E-F). In agreement, *MIR155,* shown to favor *PTGES2* expression [49], was also upregulated suggesting its role as indirect positive regulator of prostaglandin E synthase (*PTGES2/3*) expression in MCs (Figure 6F-G).

Taken together these results show that activated Teff cells induce in MCs a specific genetic program allowing them to produce a vast array of chemokines, cytokines and eicosanoid mediators.

# 4 Discussion

We and others have shown that MCs are implicated in autoinflammatory disorders such as psoriasis, acne, multiple sclerosis or inflammatory bowel diseases [13, 14, 17]. While a Th cell-MC crosstalk was often reported in these $CD4^+$ T cell driven pathologies, a comprehensive view of the impact of Teff cells on MCs is still missing.

MCs are tissue-resident cells uneasy to study due to both the difficulty to isolate them from tissues and isolation procedures altering their functionalities [50]. To decipher direct interaction between MCs and Teff cells, we used an *in vitro* coculture system. Although this system does not recapitulate the *in vivo* complexity of the multiple cell-cell interactions, it nevertheless has the advantage to allow a comprehensive study of potential interaction between $CD4^+$ Teff cells and MCs and to define $CD4^+$ T cell "help" provided to MCs. We used peripheral-blood-derived primary human MCs which are transcriptionally close to human tissue-resident MCs [51] and memory $CD4^+$ T cells from peripheral blood of healthy donors expected to be recruited in inflamed tissues and interact with MCs. To mimic $CD4^+$ T cell restimulation via TCR, memory $CD4^+$ T cells were stimulated with anti-CD3/CD28 coated beads. This antigen-independent system eliminates the need of professional antigen presenting cells in the coculture and provides a non-polarizing canonical T cell stimulation.

We analyzed gene expression induced by activated Teff cells and by two key MC stimuli (IgE/Ag and IL-33) for comparison. Unsupervised analysis clustering genes based on their expression profiles (WGCNA) indicated that an important gene module (independent of classical IgE/Ag and IL33 *stimuli*) establishing a network of highly wired genes is associated to interaction with activated Teff cells. This module is strongly related to IFN-$\gamma$ response. Subsequent analysis of DEGs between MC cocultured with activated or resting $CD4^+$ T cells showed that a majority of the yellow module genes are upregulated upon interaction with activated Teff cells. They constitute a substantial part of the transcriptomic program induced in MC by Teff cells. Among them, we found genes related to antigen presentation to $CD4^+$ T cells (MHC-class II and costimulation molecules) as well as antigen processing (Invariant chain (CD74), cathepsins S, O and L, HLA-DO), in agreement with our previous reports showing that IFN-$\gamma$ induces antigen presentation ability in MCs [17, 20. We show here that activated CD4+ Teff cells provide non-cognate help to MCs endowing them with the ability to

play the role of APC for CD4+ memory T cells. We can assume that IFN-□ produced by activated memory CD4+ T cell polyclonal population is involved in the acquisition of this function by MCs. Surprisingly, MCs also upregulated a spectrum of genes involved in Ag cross-presentation (coding for Cathepsins S and L, TAP1, TAP2, ERAP1, ERAP2, PDIA3 and NCF1, see table S2 column remarks) and antigen presentation by MHC-I molecules. These genes are also known to be induced by IFN-g. MC cognate interaction with CD8+ T cells {Stelekati, 2009 #530, 52] and MC ability to process bacterial Ags through a phagocytic route for class I MHC presentation to T cells [53] were previously reported but this phenomenon remains poorly documented. This echoes the help given by Th cells to DCs licensing them with the ability to cross-present Ag to $CD8^+$ T cells [54, 55]. However, whether MCs could process exogenous Ag to present them via MHC class I molecules remains to be investigated. Butyrophilin 3A isoforms and notably BTN3A1 (CD277) coding gene are upregulated in $MC^{Teff}$. These molecules belong to the B7 family and are involved in the TCR-dependent activation of Vγ9Vδ2 T cells by phosphoantigens [56]. Moreover, we found the endothelial cell protein C receptor (CD201) coding gene *PROCR* upregulated in $MC^{Teff}$. This non-conventional MHC class I-like antigen presentation molecule was shown to promote MC/γδ T cell immune synapse formation and γδ T cell activation and proliferation upon viral infection in mice [15].

We and others previously reported that MC express costimulation molecules either at steady state or following stimulation with LPS, viruses or IFN-γ such as CD80, CD86, OX40L or ICOS-L [16, 20, 52, 57]. Here, we extended this notion by showing that Teff cells induce several costimulatory checkpoint molecules in human MCs such as CD80, CD70, CD137L, SLAM Family Members 1,5 and 8, Galectin 9, PDL1 and PDL2 indicating that $MC^{Teff}$ might also provide a rich array of costimulatory signals to different T lymphocyte subsets. Moreover, the upregulation of genes coding for CD70, BAFF (TNFSF13B) and TRAIL (TNFSF10) could also involve $MC^{Teff}$ in the modulation of B cell responses.

Teff cells also induce the expression in MCs of several key factors dedicated to T cell functions. CXCL9, CXCL10 and CXCL11 allow the recruitment of $CXCR3^+$ Th cells and CTL into the inflammatory site and may influence Th cell orientation [58] while CCL20 attracts $CCR6^+$ Th17 cells. IL-7 and IL-15 participate to memory T cell homeostasis. Altogether, our results suggest that $CD4^+$ Teff cells license MCs with the ability to attract and restimulate (possibly in an Ag-dependent manner) $CD4^+$ or $CD8^+$ T cells in tissues. In line with our observations, increased density of activated MCs within inflamed tissues has been reported in a number of T-cell mediated inflammatory diseases such as IBD, multiple sclerosis, sarcoidosis, contact hypersensitivity, acne and psoriasis [14, 17, 59, 60]. $MC^{Teff}$ DEGs gene ontology and overlapping analysis with GWAS data indicate that upregulated genes in $MC^{Teff}$

are associated to IMID. Moreover, $MC^{Teff}$ upregulate genes coding for secreted inflammatory mediators such as pentraxin3 (PTX3), the chemokines CCL1, CCL3, CCL4 and CCL5 and the cytokines GM-CSF, M-CSF, IL-32, IL-6, TNF, lymphotoxin alpha, amphiregulin and oncostatin M (OSM). OSM was previously reported to be induced in mouse MCs by activated T cells [26] and involved in IBD [61] and sarcoidosis [62]. Thus, a deleterious crosstalk between MCs and autoreactive T cells might operate in IMID.

$MC^{Teff}$ upregulate complement components, Pentraxin 3 and several antiviral protein-coding genes such as *OAS2, OAS3, APOBEC3G*, *IFIT1, RSAD2, IFITM, PML, PARP9* indicating that $CD4^+$ T cell help could reinforce MC antimicrobial capabilities. Regarding degranulation, we did not observe degranulated MCs upon coculture with activated Teff cells in standard assays but an enhancement of FcεRI-dependent degranulation as previously reported in mouse system [20, 63].

Several MC functions potentially elicited by $CD4^+$ Teff cells (antigen presentation, antimicrobial defense, inflammatory mediator production) are known to be associated to IFN-γ stimulation. To go further, we retrieved IFN-γ-induced genes by interrogating public database cytosig (that combines multiple published dataset) and IFN-γ-induced genes in MCs according to Okumura et al. [64] and observed an important overlap with the genes we found upregulated in $MC^{Teff}$ (Figure S7 and table S3). Moreover, among candidate transcription factors that regulate these genes (Table S1), many of them are related to IFN-γ signaling such as IRF1, STAT-1, STAT-2 and IRF9 [65, 66]. It is tempting to speculate that IFN-γ induces the expression of a large panel of genes in $MC^{Teff}$ either via STAT-1 homodimer that targets ISG (interferon-stimulated gene) harboring gamma interferon-activated sites (GAS) or via IRF1 that targets genes harboring the interferon-stimulated response element (ISRE) or IRF-responsive element (IRE) [65-67]. In line with other reports [10], our analysis suggests that IFN-γ is a key memory-T-cell-derived stimulus (but not the only one) in MC help and that $MC^{Teff}$ reinforce IFN-γ signaling loop by upregulating the expression of *IFNG, STAT1, STAT2* and *JAK2* genes. These results raise questions about the impact of different $CD4^+$ Teff subsets on MCs. While the effect of IFN-γ produced by Th1 lymphocytes is clearly apparent here, it would be interesting to reproduce this study using different subsets of lymphocytes such as Th1, Th2, Th17 and Treg, to analyze whether each subset, taken separately, influences particular MC functions. Nevertheless, our study shows that, with an *ex vivo* memory $CD4^+$ T cell polyclonal population, activated $CD4^+$ lymphocytes broaden the range of MC functions.

Regarding eicosanoids production by MCs, Teff cells induce COX-dependent prostaglandin production ($PGE_2$, $PGD_2$) by MCs without *COX-2* upregulation. According to RNAseq

analysis, $MC^{Teff}$ expressed the cPGES $PGE_2$ synthase (encoded by *PTGES3*), known to be associated to COX-1 [68] and not the classical inducible microsomal mPGES1 $PGE_2$ synthase-1 (*PTGES*) metabolizing the $PGH_2$ produced by COX-2. $MC^{Teff}$ downregulated genes involved in the catabolism of $PGE_2$ (human prostaglandin reductases *PTGR1* and *PTGR2*) and upregulated Mir155 shown to favor *PTGES2* expression [49]. Thus, Teff cells might drive MC prostaglandin production through a peculiar way, that impedes the decay of homeostatic $PGE_2$ leading to its accumulation.

In this study, we showed a rich network of communication between Th cells and MC driven by multiple signaling cues. Teff cells display an adjuvant effect on MCs to perform multiple effector functions such as antigen presentation and production of inflammatory (cytokines, chemokines, eicosanoids) or antimicrobial molecules thereby, making them more prone to mount defense responses against pathogens and reactivate Ag-experienced T cells. Early activation of MCs by activated $CD4^+$ T cells might help to facilitate the initiation of immune response despite low PRR-dependent stimulation during the stealth phase of infections.

# 5 Data and code availability

RNA-seq data have been deposited at the NCBI SRA database and are publicly available as of the date of publication (GSE235240). This paper does not report original code. Any additional information required to reanalyze the data reported in this paper is available from the lead contact upon request.

# 6 ACKNOWLEDGMENTS

This work was supported by grants from the Laboratoire d'Excellence Toulouse Cancer (TOUCAN) (contract ANR11-LABEX) and from the Ligue Nationale contre le Cancer (Equipe labellisée 2018). E.L. was supported by fellowships from the French Ministry of Education and Research and from Ligue Nationale contre le Cancer. N.C is a recipient of the grant from ANR (ANR-18-CE14-0039-01). We thank the CRCT and Infinity core facilities for assistance. We gratefully acknowledge the Toulouse INSERM Metatoul-Lipidomique Core Facility-MetaboHub ANR-11-INBS-010, where lipidomic analysis were performed, and the platform Aninfimip, an EquipEx (‘Equipement d’Excellence’) supported by the French government through the Investments for the Future program (ANR-11-EQPX-0003).

# 7 AUTHORSHIP

Conceptualization: E.E. and N.C; Data curation—formal analysis: E.E, Investigation: E.E., E.L., C.P. and L.B; Writing – Original draft: E.E., N.C. and G.D.; Visualization: E.E, N.C. and L.B.; Supervision E.E and N.C; Project Administration/oversight: S.V., E.E., N.C. and G.D.

# 8 DISCLOSURES

The authors declare no conflicts of interest.

# 9 References


1. Halova, I., Ronnberg, E., Draberova, L., Vliagoftis, H., Nilsson, G. P., Draber, P. (2018) Changing the threshold-Signals and mechanisms of mast cell priming. Immunol Rev 282, 73-86.
2. Valent, P., Akin, C., Hartmann, K., Nilsson, G., Reiter, A., Hermine, O., Sotlar, K., Sperr, W. R., Escribano, L., George, T. I., et al. (2020) Mast cells as a unique hematopoietic lineage and cell system: From Paul Ehrlich's visions to precision medicine concepts. Theranostics 10, 10743-10768.
3. Galli, S. J., Gaudenzio, N., Tsai, M. (2020) Mast Cells in Inflammation and Disease: Recent Progress and Ongoing Concerns. Annu Rev Immunol 38, 49-77.
4. Espinosa, E. and Valitutti, S. (2018) New roles and controls of mast cells. Curr Opin Immunol 50, 39-47.
5. Dudeck, A., Koberle, M., Goldmann, O., Meyer, N., Dudeck, J., Lemmens, S., Rohde, M., Roldan, N. G., Dietze-Schwonberg, K., Orinska, Z., et al. (2019) Mast cells as protectors of health. J Allergy Clin Immunol 144, S4-S18.
6. Strutt, T. M., McKinstry, K. K., Dibble, J. P., Winchell, C., Kuang, Y., Curtis, J. D., Huston, G., Dutton, R. W., Swain, S. L. (2010) Memory CD4+ T cells induce innate responses independently of pathogen. Nat Med 16, 558-64, 1p following 564.
7. Wakim, L. M., Gebhardt, T., Heath, W. R., Carbone, F. R. (2008) Cutting edge: local recall responses by memory T cells newly recruited to peripheral nonlymphoid tissues. J Immunol 181, 5837-41.
8. McLachlan, J. B., Catron, D. M., Moon, J. J., Jenkins, M. K. (2009) Dendritic cell antigen presentation drives simultaneous cytokine production by effector and regulatory T cells in inflamed skin. Immunity 30, 277-88.
9. Ruterbusch, M., Pruner, K. B., Shehata, L., Pepper, M. (2020) In Vivo CD4(+) T Cell Differentiation and Function: Revisiting the Th1/Th2 Paradigm. Annu Rev Immunol 38, 705-725.
10. Soudja, S. M., Chandrabos, C., Yakob, E., Veenstra, M., Palliser, D., Lauvau, G. (2014) Memory-T-cell-derived interferon-gamma instructs potent innate cell activation for protective immunity. Immunity 40, 974-88.
11. McDaniel, M. M., Meibers, H. E., Pasare, C. (2021) Innate control of adaptive immunity and adaptive instruction of innate immunity: bi-directional flow of information. Curr Opin Immunol 73, 25-33.
12. Finlay, C. M., Parkinson, J. E., Zhang, L., Chan, B. H. K., Ajendra, J., Chenery, A., Morrison, A., Kaymak, I., Houlder, E. L., Murtuza Baker, S., et al. (2023) T helper 2 cells control monocyte to tissue-resident macrophage differentiation during nematode infection of the pleural cavity. Immunity 56, 1064-1081.e10.

13. Russi, A. E., Walker-Caulfield, M. E., Guo, Y., Lucchinetti, C. F., Brown, M. A. (2016) Meningeal mast cell-T cell crosstalk regulates T cell encephalitogenicity. Journal of autoimmunity 73, 100-10.
14. Eliasse, Y., Leveque, E., Garidou, L., Battut, L., McKenzie, B., Nocera, T., Redoules, D., Espinosa, E. (2021) IL-17(+) Mast Cell/T Helper Cell Axis in the Early Stages of Acne. Frontiers in immunology 12, 740540.
15. Mantri, C. K. and St. John, A. L. (2019) Immune synapses between mast cells and γδ T cells limit viral infection. The Journal of Clinical Investigation 129, 1094-1108.
16. Kashiwakura, J., Yokoi, H., Saito, H., Okayama, Y. (2004) T cell proliferation by direct cross-talk between OX40 ligand on human mast cells and OX40 on human T cells: comparison of gene expression profiles between human tonsillar and lung-cultured mast cells. J Immunol 173, 5247-57.
17. Gaudenzio, N., Laurent, C., Valitutti, S., Espinosa, E. (2013) Human mast cells drive memory CD4+ T cells toward an inflammatory IL-22+ phenotype. J Allergy Clin Immunol 131, 1400-7 e11.
18. Nakae, S., Suto, H., Kakurai, M., Sedgwick, J. D., Tsai, M., Galli, S. J. (2005) Mast cells enhance T cell activation: Importance of mast cell-derived TNF. Proc Natl Acad Sci U S A.
19. Lotfi-Emran, S., Ward, B. R., Le, Q. T., Pozez, A. L., Manjili, M. H., Woodfolk, J. A., Schwartz, L. B. (2018) Human mast cells present antigen to autologous CD4(+) T cells. J Allergy Clin Immunol 141, 311-321 e10.
20. Gaudenzio, N., Espagnolle, N., Mars, L. T., Liblau, R., Valitutti, S., Espinosa, E. (2009) Cell-cell cooperation at the T helper cell/mast cell immunological synapse. Blood 114, 4979-88.
21. Mekori, Y. A. and Hershko, A. Y. (2012) T cell-mediated modulation of mast cell function: heterotypic adhesion-induced stimulatory or inhibitory effects. Frontiers in immunology 3, 6.
22. Shefler, I., Mekori, Y. A., Mor, A. (2008) Stimulation of human mast cells by activated T cells leads to N-Ras activation through Ras guanine nucleotide releasing protein 1. J Allergy Clin Immunol 122, 1222-5.
23. Shefler, I., Pasmanik-Chor, M., Kidron, D., Mekori, Y. A., Hershko, A. Y. (2013) T cell-derived microvesicles induce mast cell production of IL-24: Relevance to inflammatory skin diseases. J Allergy Clin Immunol.
24. Stopfer, P., Mannel, D. N., Hehlgans, T. (2004) Lymphotoxin-beta receptor activation by activated T cells induces cytokine release from mouse bone marrow-derived mast cells. J Immunol 172, 7459-65.
25. Inamura, N., Mekori, Y. A., Bhattacharyya, S. P., Bianchine, P. J., Metcalfe, D. D. (1998) Induction and enhancement of Fc(epsilon)RI-dependent mast cell degranulation following coculture with activated T cells: dependency on ICAM-1- and leukocyte function-associated antigen (LFA)-1-mediated heterotypic aggregation. J Immunol 160, 4026-33.
26. Salamon, P., Shoham, N. G., Puxeddu, I., Paitan, Y., Levi-Schaffer, F., Mekori, Y. A. (2008) Human mast cells release oncostatin M on contact with activated T cells: possible biologic relevance. J Allergy Clin Immunol 121, 448-455 e5.
27. Le Faouder, P., Baillif, V., Spreadbury, I., Motta, J. P., Rousset, P., Chene, G., Guigne, C., Terce, F., Vanner, S., Vergnolle, N., et al. (2013) LC-MS/MS method for rapid and concomitant quantification of pro-inflammatory and pro-resolving polyunsaturated fatty acid metabolites. J Chromatogr B Analyt Technol Biomed Life Sci 932, 123-33.
28. Liao, Y., Smyth, G. K., Shi, W. (2019) The R package Rsubread is easier, faster, cheaper and better for alignment and quantification of RNA sequencing reads. Nucleic Acids Res 47, e47.
29. Love, M. I., Huber, W., Anders, S. (2014) Moderated estimation of fold change and dispersion for RNA-seq data with DESeq2. Genome Biol 15, 550.

30. Gu, Z., Eils, R., Schlesner, M. (2016) Complex heatmaps reveal patterns and correlations in multidimensional genomic data. Bioinformatics 32, 2847-2849.
31. Yu, G. and He, Q.-Y. (2016) ReactomePA: an R/Bioconductor package for reactome pathway analysis and visualization. Molecular BioSystems 12, 477-479.
32. Langfelder, P. and Horvath, S. (2008) WGCNA: an R package for weighted correlation network analysis. BMC Bioinformatics 9, 559.
33. Sollis, E., Mosaku, A., Abid, A., Buniello, A., Cerezo, M., Gil, L., Groza, T., Güneş, O., Hall, P., Hayhurst, J., et al. (2023) The NHGRI-EBI GWAS Catalog: knowledgebase and deposition resource. Nucleic Acids Res 51, D977-d985.
34. Horvath, S. and Dong, J. (2008) Geometric interpretation of gene coexpression network analysis. PLoS Comput Biol 4, e1000117.
35. Keenan, A. B., Torre, D., Lachmann, A., Leong, A. K., Wojciechowicz, M. L., Utti, V., Jagodnik, K. M., Kropiwnicki, E., Wang, Z., Ma'ayan, A. (2019) ChEA3: transcription factor enrichment analysis by orthogonal omics integration. Nucleic Acids Research 47, W212-W224.
36. Sjöstedt, E., Zhong, W., Fagerberg, L., Karlsson, M., Mitsios, N., Adori, C., Oksvold, P., Edfors, F., Limiszewska, A., Hikmet, F., et al. (2020) An atlas of the protein-coding genes in the human, pig, and mouse brain. Science 367.
37. Szklarczyk, D., Gable, A. L., Nastou, K. C., Lyon, D., Kirsch, R., Pyysalo, S., Doncheva, N. T., Legeay, M., Fang, T., Bork, P., et al. (2020) The STRING database in 2021: customizable protein–protein networks, and functional characterization of user-uploaded gene/measurement sets. Nucleic Acids Research 49, D605-D612.
38. Gillespie, M., Jassal, B., Stephan, R., Milacic, M., Rothfels, K., Senff-Ribeiro, A., Griss, J., Sevilla, C., Matthews, L., Gong, C., et al. (2021) The reactome pathway knowledgebase 2022. Nucleic Acids Research 50, D687-D692.
39. Chen, L. and Flies, D. B. (2013) Molecular mechanisms of T cell co-stimulation and co-inhibition. Nature Reviews Immunology 13, 227-242.
40. Sharpe, A. H. (2017) Introduction to checkpoint inhibitors and cancer immunotherapy. Immunological Reviews 276, 5-8.
41. Barnaba, V., Watts, C., de Boer, M., Lane, P., Lanzavecchia, A. (1994) Professional presentation of antigen by activated human T cells. Eur J Immunol 24, 71-5.
42. Lanzavecchia, A., Roosnek, E., Gregory, T., Berman, P., Abrignani, S. (1988) T cells can present antigens such as HIV gp120 targeted to their own surface molecules. Nature 334, 530-2.
43. Kappler, J., Kotzin, B., Herron, L., Gelfand, E. W., Bigler, R. D., Boylston, A., Carrel, S., Posnett, D. N., Choi, Y., Marrack, P. (1989) V beta-specific stimulation of human T cells by staphylococcal toxins. Science 244, 811-3.
44. Kupfer, A., Mosmann, T. R., Kupfer, H. (1991) Polarized expression of cytokines in cell conjugates of helper T cells and splenic B cells. Proceedings of the National Academy of Sciences 88, 775-779.
45. Huse, M., Lillemeier, B. F., Kuhns, M. S., Chen, D. S., Davis, M. M. (2006) T cells use two directionally distinct pathways for cytokine secretion. Nat Immunol 7, 247-55.
46. LaMere, S. A., Thompson, R. C., Meng, X., Komori, H. K., Mark, A., Salomon, D. R. (2017) H3K27 Methylation Dynamics during CD4 T Cell Activation: Regulation of JAK/STAT and IL12RB2 Expression by JMJD3. J Immunol 199, 3158-3175.
47. Swaim, C. D., Scott, A. F., Canadeo, L. A., Huibregtse, J. M. (2017) Extracellular ISG15 Signals Cytokine Secretion through the LFA-1 Integrin Receptor. Mol Cell 68, 581-590 e5.
48. Xiahou, Z., Wang, X., Shen, J., Zhu, X., Xu, F., Hu, R., Guo, D., Li, H., Tian, Y., Liu, Y., et al. (2017) NMI and IFP35 serve as proinflammatory DAMPs during cellular infection and injury. Nature communications 8, 950.
49. Kim, S., Lee, E. S., Lee, E. J., Jung, J. Y., Lee, S. B., Lee, H. J., Kim, J., Kim, H. J., Lee, J. W., Son, B. H., et al. (2021) Targeted eicosanoids profiling reveals a prostaglandin reprogramming in breast Cancer by microRNA-155. J Exp Clin Cancer Res 40, 43.

50. Lorentz, A., Sellge, G., Bischoff, S. C. (2015) Isolation and characterization of human intestinal mast cells. Methods Mol Biol 1220, 163-77.
51. Cildir, G., Toubia, J., Yip, K. H., Zhou, M., Pant, H., Hissaria, P., Zhang, J., Hong, W., Robinson, N., Grimbaldeston, M. A., et al. (2019) Genome-wide Analyses of Chromatin State in Human Mast Cells Reveal Molecular Drivers and Mediators of Allergic and Inflammatory Diseases. Immunity 51, 949-965 e6.
52. Hackler, Y., Siebenhaar, F., Maurer, M., Muñoz, M. (2023) Virus-infected mast cells activate virus-specific CD8+ T cells. Scandinavian Journal of Immunology n/a, e13272.
53. Malaviya, R., Twesten, N. J., Ross, E. A., Abraham, S. N., Pfeifer, J. D. (1996) Mast cells process bacterial Ags through a phagocytic route for class I MHC presentation to T cells. J Immunol 156, 1490-6.
54. Cella, M., Scheidegger, D., Palmer-Lehmann, K., Lane, P., Lanzavecchia, A., Alber, G. (1996) Ligation of CD40 on dendritic cells triggers production of high levels of interleukin-12 and enhances T cell stimulatory capacity: T-T help via APC activation. J Exp Med 184, 747-52.
55. Smith, C. M., Wilson, N. S., Waithman, J., Villadangos, J. A., Carbone, F. R., Heath, W. R., Belz, G. T. (2004) Cognate CD4(+) T cell licensing of dendritic cells in CD8(+) T cell immunity. Nat Immunol 5, 1143-8.
56. Uldrich, A. P., Rigau, M., Godfrey, D. I. (2020) Immune recognition of phosphoantigen-butyrophilin molecular complexes by gammadelta T cells. Immunol Rev 298, 74-83.
57. Nakae, S., Suto, H., Iikura, M., Kakurai, M., Sedgwick, J. D., Tsai, M., Galli, S. J. (2006) Mast cells enhance T cell activation: importance of mast cell costimulatory molecules and secreted TNF. J Immunol 176, 2238-48.
58. Karin, N. (2020) CXCR3 Ligands in Cancer and Autoimmunity, Chemoattraction of Effector T Cells, and Beyond. Frontiers in immunology 11, 976.
59. Walker, M. E., Hatfield, J. K., Brown, M. A. (2012) New insights into the role of mast cells in autoimmunity: evidence for a common mechanism of action? Biochimica et biophysica acta 1822, 57-65.
60. Eager, K. B., Hackett, C. J., Gerhard, W. U., Bennink, J., Eisenlohr, L. C., Yewdell, J., Ricciardi, R. P. (1989) Murine cell lines stably expressing the influenza virus hemagglutinin gene introduced by a recombinant retrovirus vector are constitutive targets for MHC class I- and class II-restricted T lymphocytes. J Immunol 143, 2328-35.
61. West, N. R., Hegazy, A. N., Owens, B. M. J., Bullers, S. J., Linggi, B., Buonocore, S., Coccia, M., Görtz, D., This, S., Stockenhuber, K., et al. (2017) Oncostatin M drives intestinal inflammation and predicts response to tumor necrosis factor-neutralizing therapy in patients with inflammatory bowel disease. Nat Med 23, 579-589.
62. Guber, A., Jawad, A. Q., Salomon, P., Mekori, Y. A., Shitrit, D. (2013) Oncostatin M in bronchoalveolar lavage correlates with the severity of sarcoidosis. Sarcoidosis Vasc Diffuse Lung Dis 30, 194-200.
63. Bhattacharyya, S. P., Drucker, I., Reshef, T., Kirshenbaum, A. S., Metcalfe, D. D., Mekori, Y. A. (1998) Activated T lymphocytes induce degranulation and cytokine production by human mast cells following cell-to-cell contact. J Leukoc Biol 63, 337-41.
64. Okumura, S., Kashiwakura, J., Tomita, H., Matsumoto, K., Nakajima, T., Saito, H., Okayama, Y. (2003) Identification of specific gene expression profiles in human mast cells mediated by Toll-like receptor 4 and FcepsilonRI. Blood 102, 2547-54.
65. Michalska, A., Blaszczyk, K., Wesoly, J., Bluyssen, H. A. R. (2018) A Positive Feedback Amplifier Circuit That Regulates Interferon (IFN)-Stimulated Gene Expression and Controls Type I and Type II IFN Responses. Frontiers in immunology 9.
66. Platanitis, E., Demiroz, D., Schneller, A., Fischer, K., Capelle, C., Hartl, M., Gossenreiter, T., Müller, M., Novatchkova, M., Decker, T. (2019) A molecular switch

from STAT2-IRF9 to ISGF3 underlies interferon-induced gene transcription. Nature communications 10, 2921.
67. Rosain, J., Neehus, A.-L., Manry, J., Yang, R., Le Pen, J., Daher, W., Liu, Z., Chan, Y.-H., Tahuil, N., Türel, Ö., et al. (2023) Human IRF1 governs macrophagic IFN-γ immunity to mycobacteria. Cell 186, 621-645.e33.
68. Murakami, M. and Kudo, I. (2006) Prostaglandin E synthase: a novel drug target for inflammation and cancer. Curr Pharm Des 12, 943-54.

# Figure legends

**Figure 1. Activated CD4$^+$ T cells induce specific gene expression program in MCs**

MCs were activated by IL-33 or IgE anti-DNP/DNP-BSA or cocultured with unstimulated (+$T_{CTRL}$) or anti-CD3/CD28 stimulated CD4$^+$ memory T cells (+$T_{ACT}$). MCs were next sorted by FACS and subjected to RNA sequencing. (A) Experimental setup. (B) PCA analysis of sample relationship (n=4 donors). The percent of variance explained by each component is reported. (C) 500 most significantly DEGs between the different stimulation conditions and control condition (Unstimulated MCs) were plotted in a heatmap. Regularized-logarithm transformed counts values (DESeq2, rlog function) were mean-centered and scaled for each gene. Hierarchical clustering of DEGs and samples was based on Euclidean distance using complete linkage function. Each column corresponds to one sample with indicated donor and stimulation condition and each row corresponds to a specific gene. (D) Number of DEG distribution between the different stimulation conditions and control condition according to fold change expression. (E) Proportional-area Venn diagrams showing the overlap of DEGs ($log_2$ fold change ≥ 1; adjusted p value (FDR) ≤ 0.01) in activated MCs (+IgE/Ag, blue; +IL-33, yellow; +$T_{ACT}$, red) versus resting MCs.

**Figure 2. MC gene module uniquely associated with Teff cell interaction**

Gene clustering according to their expression profile across all stimulation conditions by Weighted gene co-expression network analysis. (A) Gene dendrogram generated on the Topological Overlap Dissimilarity matrix: each branch of the dendrogram corresponds to a module of highly interconnected genes. Colors represent module membership clustered by the dynamic tree cut method. (B) Heatmap of module eigengene (ME) values across stimulation conditions. The module eigengenes represent the first principal component of a given module (representative of the gene expression profiles in a module) and allow to figure out which module is associated with which stimulation condition. Only yellow module shows a high positive ME value only in +$T_{ACT}$ condition. (C) Reactome pathway enrichment analysis

based on the yellow module genes showing a high module membership (i.e. eigengene-based connectivity $k_{ME}$) >0.8. Shown are the top 4 non-redundant pathways and associated genes. Expression fold changes ($+T_{ACT}$ vs unstimulated condition) are color scaled. (D) Transcription factor target over-representation analysis performed on yellow module genes ($k_{ME}$>0.8) using ChEA3 database. Transcription factors were ranked according to their score obtained by the TopRank method integrating the best scaled rank of each TF across all ChEA3 libraries tested. Bars represent score and color range indicates the number of genes targeted by each transcription factor.

**Figure 3. Gene expression change induced by Teff cells in MCs ($MC+T_{ACT}$ vs $MC+T_{CTRL}$)**

(A) Volcano plot showing the P-adjusted value (-log10-transformed) as a function of the fold-change ($log_2$-transformed) from $MC+T_{ACT}$ relative to $MC+T_{CTRL}$. Genes with $|log_2$ fold change$| > 1$ and FDR < 0.01 (significantly differentially expressed genes) are in red, genes with $|log_2$ fold change$| > 1$ but FDR ≥ 0.01 are in green, genes with $|log_2$ fold change$| \leq 1$ but FDR < 0.01 are in blue, and the rest are in grey. (B) Main STRING PPI network generated from upregulated protein-coding DEGs (with confidence score greater than 0.7) and top 5 subnetworks identified by Markov Clustering (MCL) with inflating score of 3 using Cytoscape. Proteins are presented as nodes connected by lines whose thickness represents the confidence level, colors indicate the MCL subnetworks and form indicates genes found (square) or not (circle) in the WGCNA yellow module. For each subnetwork, the main result from STRING pathway-enrichment analysis (GO biological process) is indicated. (C) Gene set enrichment analysis (Reactome pathways) of upregulated DEGs (FC>2 and FDR<0.01) between $MC+T_{ACT}$ vs $MC+T_{CTRL}$ conditions (FDR<0.01). Shown are the top 15 enriched pathways (ranked by p-adjusted value). Each line represents a Reactome pathway, the point size indicates the number of DEGs in the pathway and the color indicates the p-adjusted value. Rich factor is defined as the ratio of DEGs that are annotated in a pathway to all genes that are annotated in this pathway.

**Figure 4. Activated Teff cells endow MCs with APC capabilities**

(A) Clustered heatmap of known gene involved in immunological synapse formation (APC side) coding for HLA class II (only genes coding one HLA-DP and one HLA-DR are shown) and co-stimulation molecules. Heatmap shows the relative expression level of each gene between $MC+T_{ACT}$ vs $MC+T_{CTRL}$ conditions. Each gene expression level in $+T_{ACT}$ condition (as depicted by transcript per kilobase million, TPM) and its $log_2$ fold change expression and

associated FDR (stars indicate FDR<0.01) are also shown. Some gene symbols were replaced by more common coded protein names. CD86 was not expressed and is not represented. (B) MCs were cocultured or not with $CD4^+$ T cells for 48 hours and HLA-DR,-DP,-DQ, ICAM-1, PD-L1, CD80 expression on MC surface was analyzed by flow cytometry. Representative histograms and pooled data (depicted as % positive cells for HLA-DR, DP, DQ and CD80 or geometric mean fluorescence intensity (gMFI) fold increase over the control for ICAM-1 and PD-L1), bars represent mean ± SEM; each point represents an experiment (n= 9-17). (C) Cells from MC+$T_{ACT}$ and MC+$T_{CTRL}$ coculture conditions were pulsed or not pulsed with superantigens and incubated with CFSE-labelled resting memory $CD4^+$ T cells for 2.5 hours and immunological synapse formation was analyzed by indirect immunofluorescence staining and confocal microscopy. Two examples of typical functional immunological synapse formation (i.e. MC-$CFSE^+$ $CD4^+$ T cell conjugates exhibiting $CD4^+$ T cell polarizing IFN-γ toward superantigen loaded MC) from MC+$T_{ACT}$ condition. (D) Quantification of functional immunological synapses formed between MCs and $CFSE^+$ $CD4^+$ T cells from MC+$T_{ACT}$ and MC+$T_{CTRL}$ conditions. Each points represents the percentage of $CFSE^+$ T cells showing polarized IFN-γ production (as shown in C) among $CFSE^+$ T cells conjugated with MCs scored in a 20X field from 3 independent experiments (see examples Figure S6).

**Figure 5. Teff cells induce the secretion of proinflammatory cytokines and chemokines in MCs**

(A) 32 upregulated and expressed genes (strong or intermediate level: FC>3 and TPM>10) coding secreted proteins were mapped with STRING database and resulting PPI networks (built with high confidence level >0.7). Cytokines (blue), chemokines (purple), antimicrobial proteins (green) and others (grey). (B to D) MCs were cultured with or without CD4 memory T cells for 48h. (B) CXCL9 or CXCL10 concentrations in the culture supernatant were measured by bead-based multiplex assay (n=9). (C) Representative dot plots of CXCL9 or CXCL10 intracellular staining gated on MCs ($CD117^+$ cells) and pooled data from 6 independent experiments; bars represent mean ± SEM; each point represents an experiment. (D) IL-6, IL-1β, TNF, IL-12 and IL-23 concentrations in the culture supernatant were measured by bead-based multiplex assay. Bars represent mean ± SEM; each point represents an experiment (n=10). Friedman test followed by paired Wilcoxon signed-rank test. *$p < 0.05$, **$p < 0.01$, ***$p < 0.001$, ****$p < 0.0001$, ns not significant.

**Figure 6. Activated $CD4^+$ T cells potentiate MC degranulation and induce eicosanoid production.**

(A-B) anti-DNP IgE sensitized MCs were cocultured with $T_{ACT}$ or $T_{CTRL}$ for 48 hours and next challenged with DNP-BSA for 30 min. Degranulation was measured by CD63 exposure on the MC surface by flow cytometry (A) or by the standard β-hexosaminidase release assay (B). Representative histograms (left panel) and pooled data (mean ± SEM, n=8) (right panel) from 3 independent experiments. Two-way ANOVA with Tukey's multiple comparisons test. (C-D) MCs were cocultured with $T_{ACT}$ or $T_{CTRL}$ for 48 hours. Eicosanoids were quantified in the cell pellets by LC-MS/MS. Data are presented as box and whiskers plot (Tukey style), each point represents a MC/T cell pair (n=7 from 3 independent experiments). Friedman test and pairwise comparisons using paired Wilcoxon signed-rank test (C). MCs and $CD4^+$ T cells were FACS-sorted from $+T_{ACT}$ condition and eicosanoids were quantified in the cell pellets by LC-MS/MS. Bars represent the mean (n=6), each point represents a MC/T cell pair (D). (E) MCs were cocultured with $T_{ACT}$ separated or not with 0.4 µm transwell inserts for 48 hours. Eicosanoids were quantified in the cell supernatant by LC-MS/MS. Paired Wilcoxon signed-rank test. *$p < 0.05$, **$p < 0.01$, ***$p < 0.001$, ****$p < 0.0001$, ns not significant. (F-G) Scheme of $PGE_2$ metabolism and related genes (dashed arrows indicate indirect positive action) (F) and clustered heatmap showing the relative expression level of each MC gene between MC $+T_{ACT}$ vs MC $+T_{CTRL}$ conditions (G). Each gene expression level in $+T_{ACT}$ condition (as depicted by transcript per kilobase million, TPM) and its $\log_2$ fold change expression and associated FDR (stars indicate FDR<0.01) are also shown.

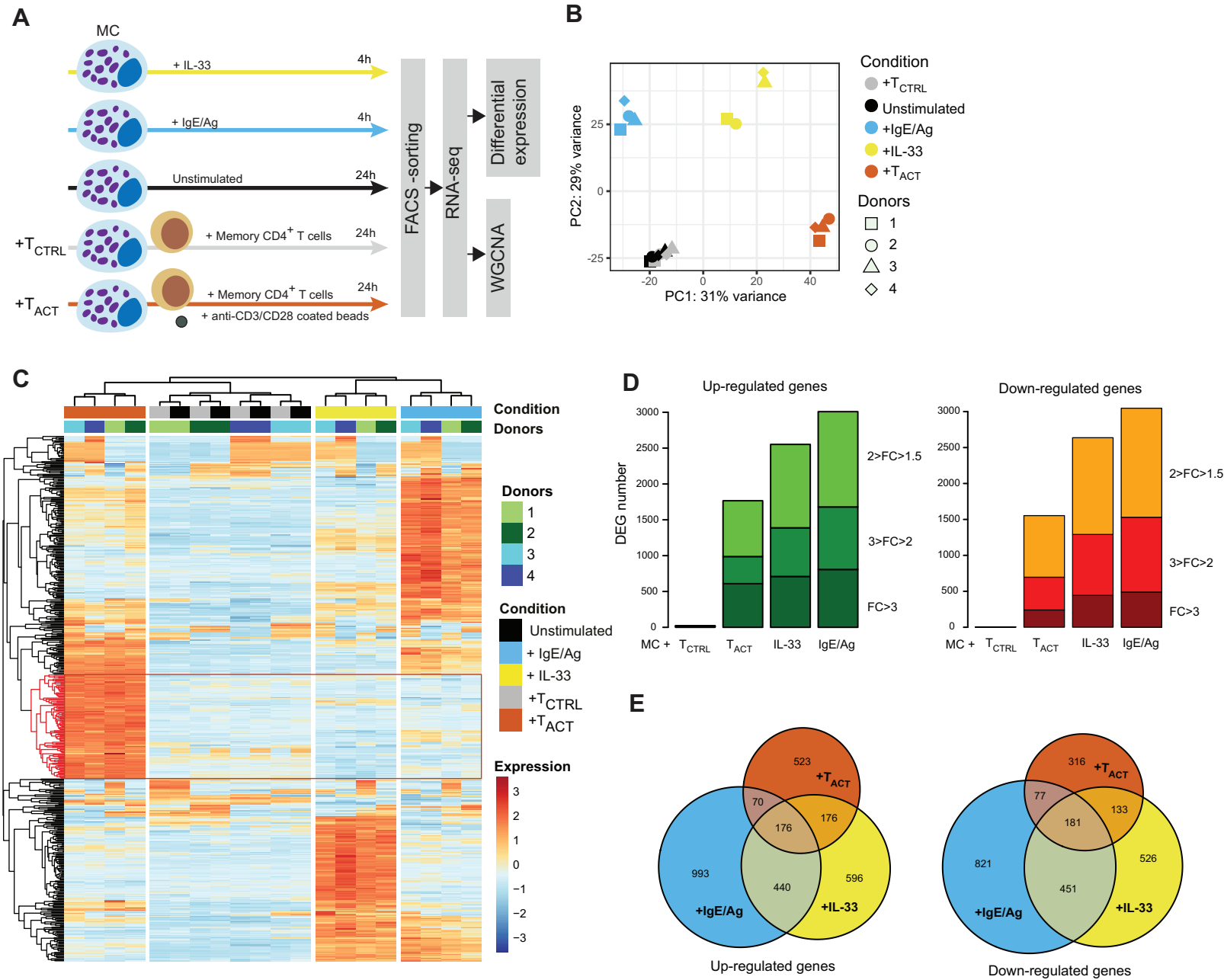
A
MC
+ IL-33
4h
+ IgE/Ag
4h
Unstimulated
24h
+T_CTRL
+ Memory CD4+ T cells
24h
+T_ACT
+ Memory CD4+ T cells
24h
+ anti-CD3/CD28 coated beads
FACS -sorting
RNA-seq
Differential expression
WGCNA
B
PC2: 29% variance
PC1: 31% variance
Condition
+T_CTRL
Unstimulated
+IgE/Ag
+IL-33
+T_ACT
Donors
1
2
3
4
C
Condition
Donors
Donors
1
2
3
4
Condition
Unstimulated
+ IgE/Ag
+ IL-33
+T_CTRL
+T_ACT
Expression
D
Up-regulated genes
Down-regulated genes
DEG number
2>FC>1.5
3>FC>2
FC>3
MC +
T_CTRL
T_ACT
IL-33
IgE/Ag
E
+T_ACT
+IgE/Ag
+IL-33
Up-regulated genes
Down-regulated genes

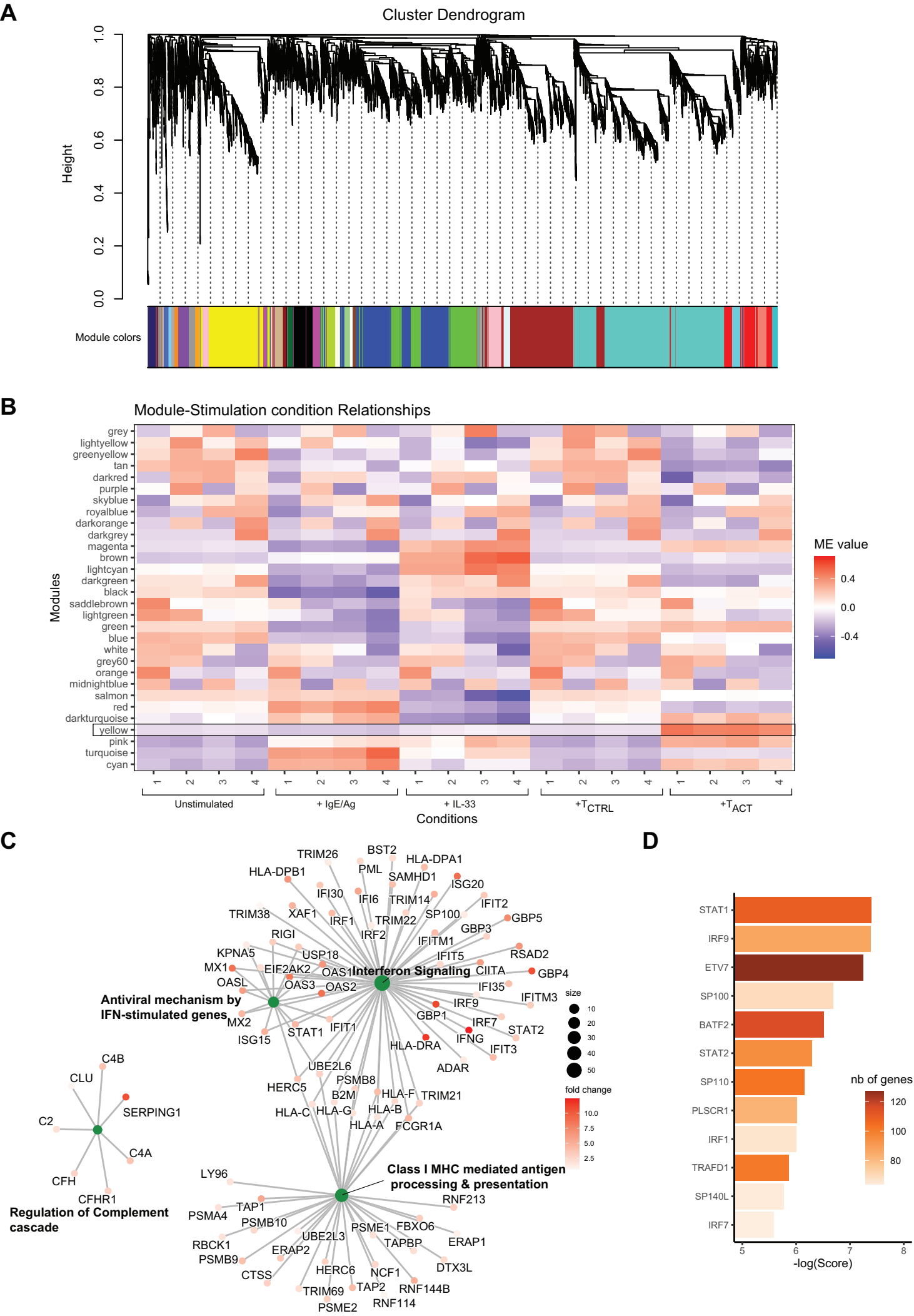
A
Cluster Dendrogram
Height
1.0
0.8
0.6
0.4
0.2
0.0
Module colors
B
Module-Stimulation condition Relationships
Modules
grey
lightyellow
greenyellow
tan
darkred
purple
skyblue
royalblue
darkorange
darkgrey
magenta
brown
lightcyan
darkgreen
black
saddlebrown
lightgreen
green
blue
white
grey60
orange
midnightblue
salmon
red
darkturquoise
yellow
pink
turquoise
cyan
1 2 3 4 1 2 3 4 1 2 3 4 1 2 3 4 1 2 3 4
Unstimulated
+ IgE/Ag
+ IL-33
+TCTRL
+TACT
Conditions
ME value
0.4
0.0
-0.4
C
Antiviral mechanism by IFN-stimulated genes
Interferon Signaling
Class I MHC mediated antigen processing & presentation
Regulation of Complement cascade
TRIM26
BST2
HLA-DPA1
HLA-DPB1
PML
SAMHD1
ISG20
IFI30
IFI6
TRIM14
IFIT2
TRIM38
XAF1
IRF1
TRIM22
SP100
GBP5
RIGI
IRF2
GBP3
IFITM1
KPNA5
USP18
IFIT5
RSAD2
MX1
EIF2AK2
OAS1
CIITA
GBP4
OASL
OAS3
OAS2
IFI35
IFITM3
MX2
ISG15
STAT1
IFIT1
GBP1
IRF9
IRF7
STAT2
IFNG
IFIT3
HLA-DRA
ADAR
UBE2L6
PSMB8
HERC5
B2M
HLA-F
TRIM21
HLA-C
HLA-G
HLA-B
HLA-A
FCGR1A
size
10
20
30
40
50
fold change
10.0
7.5
5.0
2.5
C4B
CLU
SERPING1
C2
C4A
CFH
CFHR1
LY96
RNF213
TAP1
PSMA4
PSMB10
PSME1
FBXO6
UBE2L3
TAPBP
ERAP1
RBCK1
ERAP2
PSMB9
DTX3L
CTSS
HERC6
NCF1
TRIM69
TAP2
RNF144B
PSME2
RNF114
D
STAT1
IRF9
ETV7
SP100
BATF2
STAT2
SP110
PLSCR1
IRF1
TRAFD1
SP140L
IRF7
nb of genes
120
100
80
5
6
7
8
-log(Score)

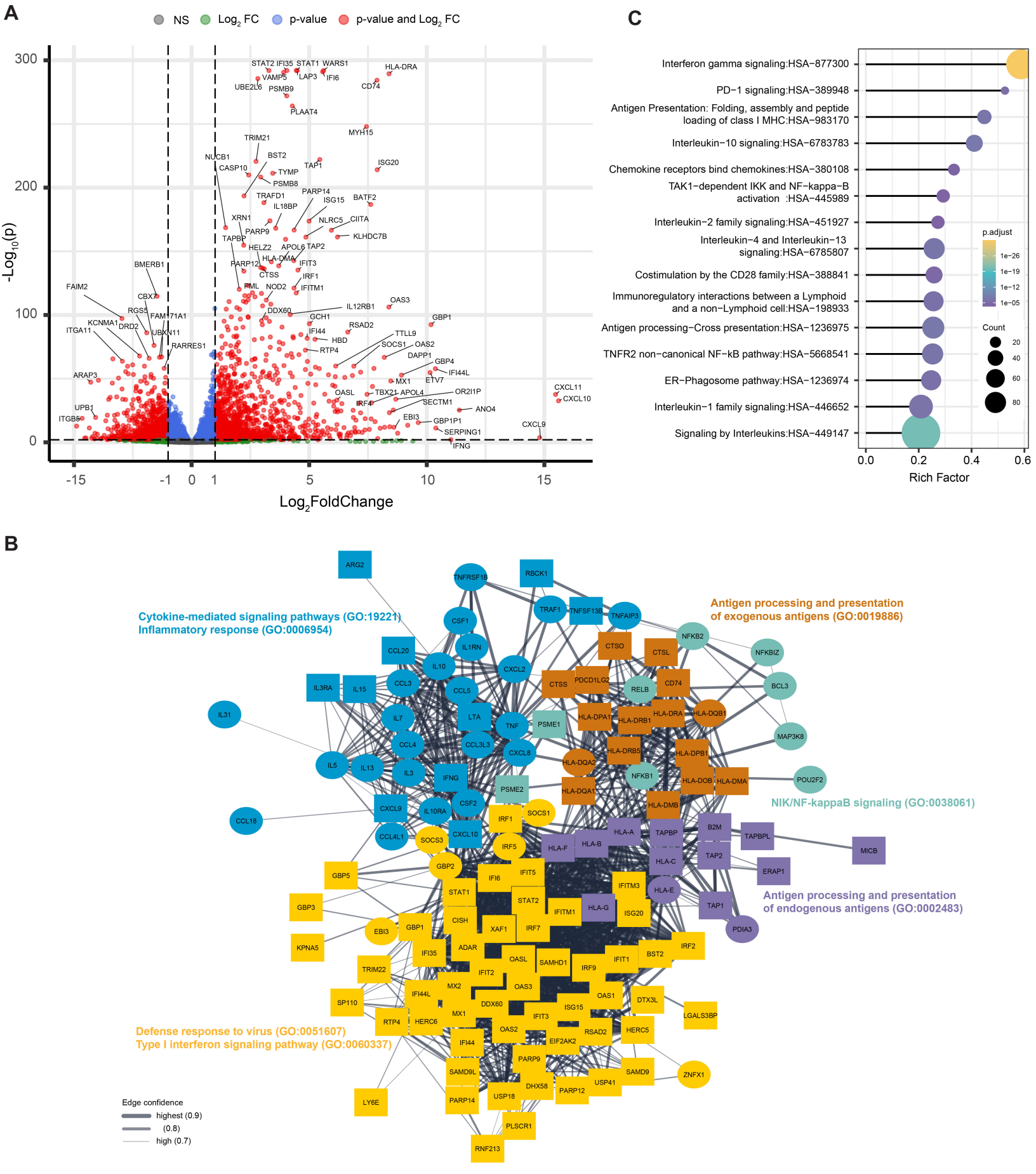
A
NS
Log2 FC
p-value
p-value and Log2 FC
-Log10(p)
Log2FoldChange
C
Interferon gamma signaling:HSA−877300
PD−1 signaling:HSA−389948
Antigen Presentation: Folding, assembly and peptide loading of class I MHC:HSA−983170
Interleukin−10 signaling:HSA−6783783
Chemokine receptors bind chemokines:HSA−380108
TAK1−dependent IKK and NF−kappa−B activation :HSA−445989
Interleukin−2 family signaling:HSA−451927
Interleukin−4 and Interleukin−13 signaling:HSA−6785807
Costimulation by the CD28 family:HSA−388841
Immunoregulatory interactions between a Lymphoid and a non−Lymphoid cell:HSA−198933
Antigen processing−Cross presentation:HSA−1236975
TNFR2 non−canonical NF−kB pathway:HSA−5668541
ER−Phagosome pathway:HSA−1236974
Interleukin−1 family signaling:HSA−446652
Signaling by Interleukins:HSA−449147
p.adjust
Count
Rich Factor
B
Cytokine-mediated signaling pathways (GO:19221)
Inflammatory response (GO:0006954)
Antigen processing and presentation of exogenous antigens (GO:0019886)
NIK/NF-kappaB signaling (GO:0038061)
Antigen processing and presentation of endogenous antigens (GO:0002483)
Defense response to virus (GO:0051607)
Type I interferon signaling pathway (GO:0060337)
Edge confidence
highest (0.9)
(0.8)
high (0.7)

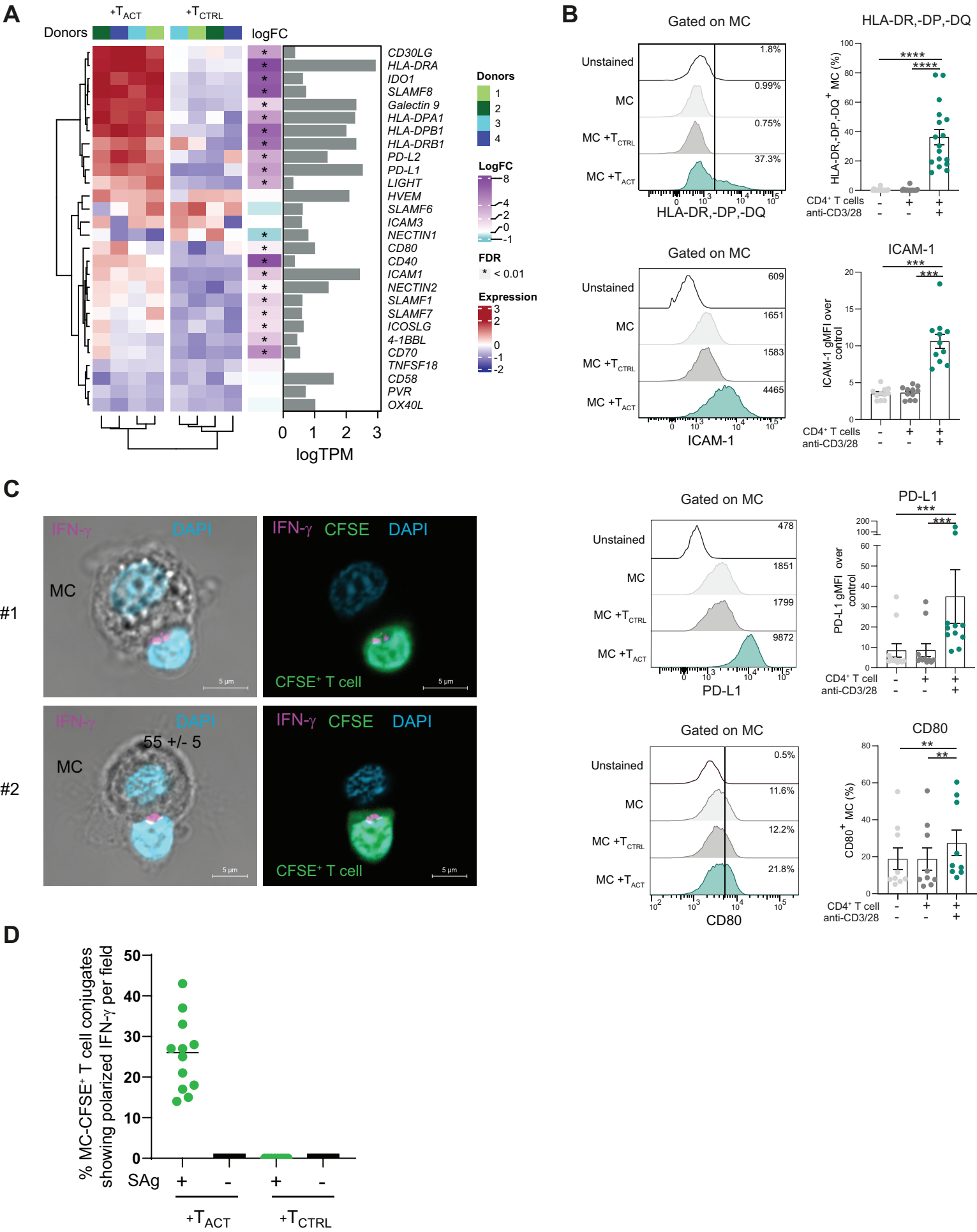
A
+T_ACT
+T_CTRL
Donors
logFC
CD30LG
HLA-DRA
IDO1
SLAMF8
Galectin 9
HLA-DPA1
HLA-DPB1
HLA-DRB1
PD-L2
PD-L1
LIGHT
HVEM
SLAMF6
ICAM3
NECTIN1
CD80
CD40
ICAM1
NECTIN2
SLAMF1
SLAMF7
ICOSLG
4-1BBL
CD70
TNFSF18
CD58
PVR
OX40L
0 1 2 3
logTPM
Donors
1
2
3
4
LogFC
8
4
2
0
-1
FDR
* < 0.01
Expression
3
2
0
-1
-2
B
Gated on MC
HLA-DR,-DP,-DQ
Unstained
MC
MC +T_CTRL
MC +T_ACT
1.8%
0.99%
0.75%
37.3%
HLA-DR,-DP,-DQ
HLA-DR,-DP,-DQ+ MC (%)
****
****
CD4+ T cells
anti-CD3/28
Gated on MC
ICAM-1
609
1651
1583
4465
ICAM-1
ICAM-1 gMFI over control
***
***
C
#1
#2
IFN-γ
DAPI
CFSE
MC
CFSE+ T cell
5 µm
55 +/- 5
Gated on MC
PD-L1
478
1851
1799
9872
PD-L1 gMFI over control
CD4+ T cell
Gated on MC
CD80
0.5%
11.6%
12.2%
21.8%
CD80+ MC (%)
**
**
D
% MC-CFSE+ T cell conjugates showing polarized IFN-γ per field
SAg
+
-
+T_ACT
+T_CTRL

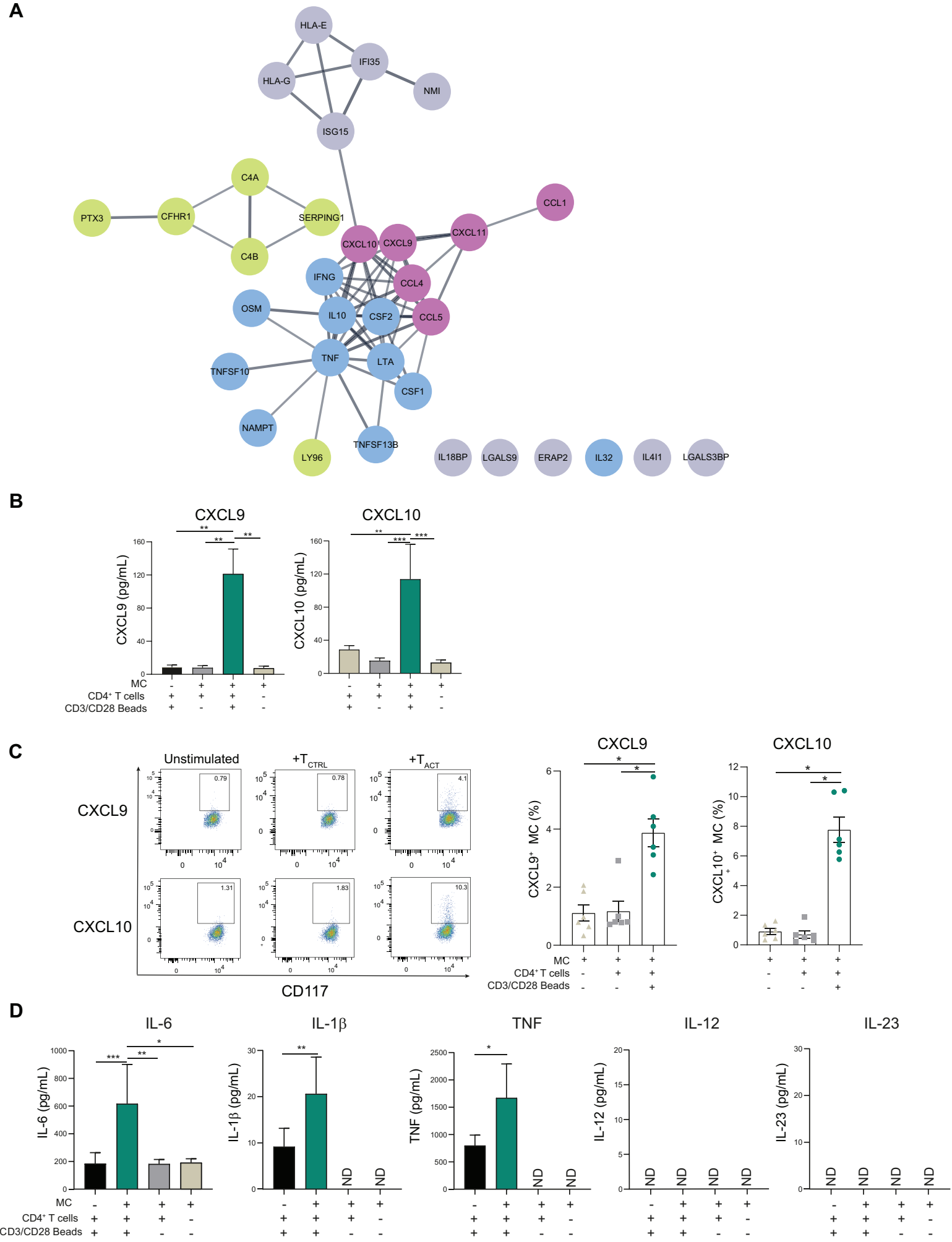
A
HLA-E
IFI35
HLA-G
NMI
ISG15
C4A
PTX3
CFHR1
SERPING1
C4B
CCL1
CXCL10
CXCL9
CXCL11
IFNG
CCL4
OSM
IL10
CSF2
CCL5
TNF
LTA
TNFSF10
CSF1
NAMPT
TNFSF13B
LY96
IL18BP
LGALS9
ERAP2
IL32
IL4I1
LGALS3BP
B
CXCL9
CXCL10
CXCL9 (pg/mL)
CXCL10 (pg/mL)
MC
CD4⁺ T cells
CD3/CD28 Beads
C
Unstimulated
+T_CTRL
+T_ACT
CXCL9
CXCL10
CD117
CXCL9⁺ MC (%)
CXCL10⁺ MC (%)
D
IL-6
IL-1β
TNF
IL-12
IL-23
IL-6 (pg/mL)
IL-1β (pg/mL)
TNF (pg/mL)
IL-12 (pg/mL)
IL-23 (pg/mL)
ND

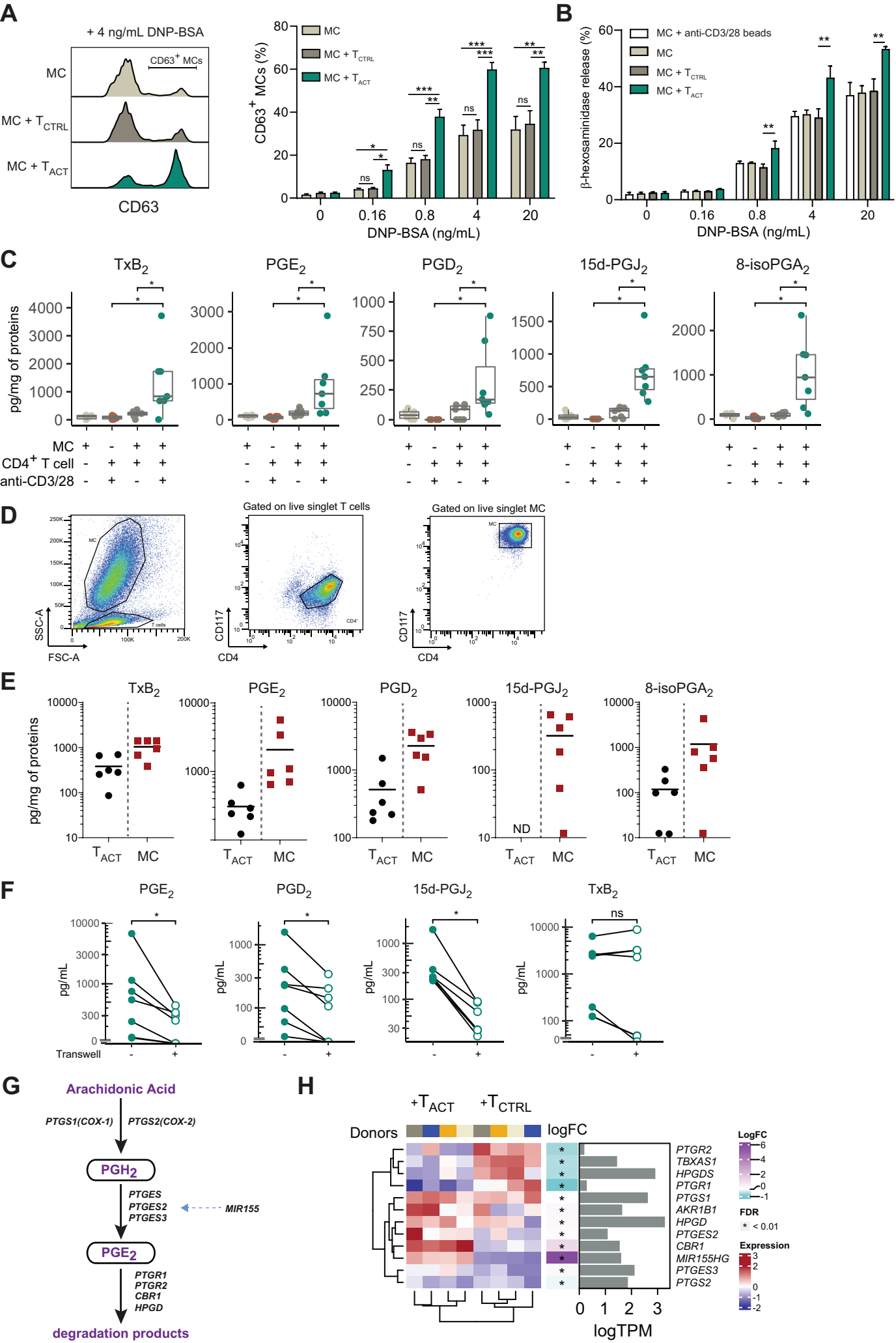
A
+ 4 ng/mL DNP-BSA
MC
MC + T_CTRL
MC + T_ACT
CD63+ MCs
CD63
CD63+ MCs (%)
DNP-BSA (ng/mL)
B
β-hexosaminidase release (%)
MC + anti-CD3/28 beads
C
TxB2
PGE2
PGD2
15d-PGJ2
8-isoPGA2
pg/mg of proteins
CD4+ T cell
anti-CD3/28
D
Gated on live singlet T cells
Gated on live singlet MC
SSC-A
FSC-A
CD117
CD4
E
ND
F
PGE2
PGD2
15d-PGJ2
TxB2
pg/mL
Transwell
G
Arachidonic Acid
PTGS1(COX-1)
PTGS2(COX-2)
PGH2
PTGES
PTGES2
PTGES3
MIR155
PGE2
PTGR1
PTGR2
CBR1
HPGD
degradation products
H
+T_ACT
+T_CTRL
Donors
logFC
PTGR2
TBXAS1
HPGDS
PTGR1
PTGS1
AKR1B1
HPGD
PTGES2
CBR1
MIR155HG
PTGES3
PTGS2
logTPM
LogFC
FDR
Expression